Eur Phys J C **44**, s02, 13–33 (2005)
Digital Object Identifier (DOI) 10.1140/epjcd/s2005-02-009-9

EPJ C direct
electronic only

Scientific Note

ATLAS sensitivity to top quark and W boson polarization in $t\bar{t}$ events

F. Hubaut[1], E. Monnier[1], P. Pralavorio[1], K. Smolek[2], V. Simak[3,4]

[1] Centre de Physique des Particules de Marseille, CNRS/IN2P3 - Univ. Méditerranée, Marseille, France
[2] Institute of Experimental and Applied Physics, Czech Technical University, Prague, Czech Republic
[3] Faculty of Nuclear Sciences and Physical Engineering, Czech Technical University, Prague, Czech Republic
[4] Institute of Physics of the Czech Academy of Sciences, Prague, Czech Republic

Received: 1 September 2005 / Revised version: 5 October 2005 /
Published online: 26 October 2005 –

Abstract. Stringent tests on top quark production and decay mechanisms are provided by the measurement of the top quark and W boson polarization. This paper presents a detailed study of these two measurements with the ATLAS detector, in the semileptonic ($t\bar{t} \to WWb\bar{b} \to l\nu j_1 j_2 b\bar{b}$) and dileptonic ($t\bar{t} \to WWb\bar{b} \to l\nu l\nu b\bar{b}$) $t\bar{t}$ channels. It is based on leading-order Monte Carlo generators and on a fast simulation of the detector. A particular attention is paid to the systematic uncertainties, which dominate the statistical errors after one LHC year at low luminosity ($10\,\mathrm{fb}^{-1}$), and to the background estimate. Combining results from both channel studies, the longitudinal component of the W polarization (F_0) can be measured with a 2% accuracy and the right-handed component (F_R, which is zero in the Standard Model) with a 1% precision with $10\,\mathrm{fb}^{-1}$. Even though the top quarks in $t\bar{t}$ pairs are not polarized, a large asymmetry is expected within the Standard Model in the like-spin versus unlike-spin pair production. A 4% precision on this asymmetry measurement is possible with $10\,\mathrm{fb}^{-1}$, after combining results from both channel studies. These promising results are converted in a sensitivity to new physics, such as tWb anomalous couplings, top decay to charged Higgs boson, or new s-channels (heavy resonance, gravitons) in $t\bar{t}$ production.

Contents

1 Introduction

Because of its high mass, intriguingly close to the electroweak symmetry breaking scale, the top quark raises interesting questions and its sector is an ideal place to look for new physics [1, 2]. Consequently, the search for non Standard Model interactions both in top quark production and decay is one of the main motivations for top quark physics. A consequence of the very high top mass is that this quark decays before it can form hadronic bound states [3]. This unique feature among quarks allows direct top spin studies, since spin properties are not washed out by hadronization and since the typical top spin-flip time is much larger than the top lifetime. Therefore, top spin polarization [4] and correlation [5] are precisely predicted by the Standard Model (SM) and reflect fundamental interactions involved in the top quark production and decay. By testing only the top decay, the W boson polarization measurement complements top spin studies, helping to disentangle the origin of new physics, if observed. Namely, the $t \to W^+b$ decay mode is responsible for 99.9% of top quark decays in the SM. Therefore, the W polarization in the top decay is unambiguously predicted by the SM and its measurement provides a direct test of the tWb vertex understanding and more particularly of its V-A structure [6, 7].

As a consequence, W polarization in top decay and top spin observables are sensitive probes of new physics in top production and decay. At the production level, a non-exhaustive list involves either anomalous $gt\bar{t}$ couplings [8,9], which naturally arise in dynamical electroweak symmetry breaking models [2] such as technicolor [10] or topcolor [11], or new interactions, as for example a strong coupling of the top quark with a heavy spin 0 resonance, such as a heavy (pseudo)scalar Higgs boson [12] as predicted e.g. by SUSY models ($gg \to H \to t\bar{t}$), or the presence of extra dimensions [13]. At the decay level, deviations from the

Standard Model can for example arise from tWb anomalous couplings, such as a V+A contribution in the vertex structure [14], or from a decay to charged Higgs boson [15].

Precise measurements of W and top polarization require a higher statistics than currently available from Tevatron data. The Large Hadron Collider (LHC) will be a top factory, producing more than 8 millions of $t\bar{t}$ events per year during its low luminosity running phase ($10^{33}\,\mathrm{cm}^{-2}\mathrm{s}^{-1}$), corresponding to an integrated luminosity of $10\,\mathrm{fb}^{-1}$. The production will occur through the $gg \to t\bar{t}$ (90%) and $q\bar{q} \to t\bar{t}$ (10%) hard processes. Depending on the W decay modes, the $t\bar{t}$ events can be classified into three channels: the semileptonic channel ($t\bar{t} \to WWb\bar{b} \to l\nu j_1 j_2 b\bar{b}$), the dileptonic channel ($t\bar{t} \to WWb\bar{b} \to l\nu l\nu b\bar{b}$) and the all hadronic channel ($t\bar{t} \to WWb\bar{b} \to j_1 j_2 j_3 j_4 b\bar{b}$). The latter will be difficult to extract from the huge QCD background and has not been considered in this work. The electroweak single top production processes, which amount to approximately one third of the $t\bar{t}$ cross-section, can also be used to measure the polarization effects, but with a lower precision [16]. They are not investigated in the following.

The goal of this paper is to evaluate the precision to which W boson and top quark polarization can be measured with the ATLAS detector, by combining results from dileptonic and semileptonic $t\bar{t}$ channels. It is organized as follows. Section 2 discusses the W boson and top quark polarization in $t\bar{t}$ events, and gives the related physics observables. Section 3 presents the event simulation, reconstruction and selection, as well as a detailed background estimate. Section 4 gives the expected ATLAS sensitivity to the W polarization, including a complete study of the systematic uncertainties. From these results, the sensitivity to the magnitude of tWb anomalous couplings that parametrize new physics is also extracted. Using the same selected events, Sect. 5 presents the expected ATLAS sensitivity to the top polarization, and to the related physics beyond the SM. Section 6 is dedicated to conclusions.

2 W boson and top quark polarization in $t\bar{t}$ events

This section presents the observables used to measure the polarization of the W boson (Sect. 2.1) and of the top quark (Sect. 2.2).

2.1 W polarization observables

There are three possible helicities for a spin-one W^+ boson, -1, 0 and +1, that will be called left-handed, longitudinal and right-handed in the following. A real W^+ in the $t \to W^+b$ decay can be produced in any of those helicity states, as sketched in Fig. 1. The corresponding probabilities are F_0, F_L and F_R, respectively, whose SM expectations at

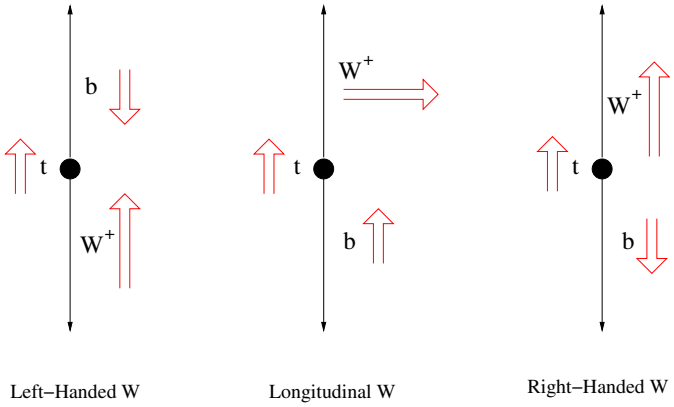

Fig. 1. Sketches of angular momentum conservation in $t \to W^+b$ decay in the top rest frame. Simple (open) arrows denote particle direction of motion (spin). As a massless b-quark must be left-handed, the rightmost plot is forbidden in the SM at tree level

tree level in the zero b-mass approximation are:

$$\begin{cases} F_0 = \dfrac{\mathrm{M}_t^2}{\mathrm{M}_t^2 + 2\mathrm{M}_W^2} = 0.703 + 0.002 \times (\mathrm{M}_t - 175) \\ F_L = \dfrac{2\mathrm{M}_W^2}{\mathrm{M}_t^2 + 2\mathrm{M}_W^2} = 0.297 - 0.002 \times (\mathrm{M}_t - 175) \\ F_R = 0.000 \end{cases} \quad (1)$$

where M_t and M_W are the top and W masses in GeV. Left and right components are inverted for W^- bosons. By definition, we have the restriction $F_0 + F_L + F_R = 1$. Since massless particles must be left-handed in the SM, right-handed W^+ bosons do not exist in the zero b-mass approximation, due to angular momentum conservation sketched in Fig. 1. Including QCD and electroweak radiative corrections, finite width corrections and non-zero b-quark mass induces small variations: $F_0 = 0.695$, $F_L = 0.304$ and $F_R = 0.001$ for $\mathrm{M}_t = 175\,\mathrm{GeV}$ [17]. Because the top quark is very heavy, F_0 is large and the top decay is the only significant source of longitudinal W bosons[1]. Deviations of F_0 from its SM value would bring into question the validity of the Higgs mechanism of the spontaneous symmetry breaking, responsible for the longitudinal degree of freedom of the massive gauge bosons. Any deviation of F_R from zero could point to a non-SM V+A admixture to the standard left-handed weak current, as for example predicted by $SU(2)_L \times SU(2)_R \times U(1)$ extensions of the SM [18].

The best way to access particle spin information is to measure the angular distribution of its decay products, thereby called spin analyzers. As an example, illustrated in Fig. 2, the charged lepton from the decay of longitudinally polarized W^+ tends to be emitted transversally to the W^+ direction, due to angular momentum conservation. Similarly, the charged lepton from a left-handed (right-handed) W^+ is preferentially emitted in the opposite (same) W^+

[1] QCD production, the only other source of real W bosons, produces nearly all W transversely polarized.

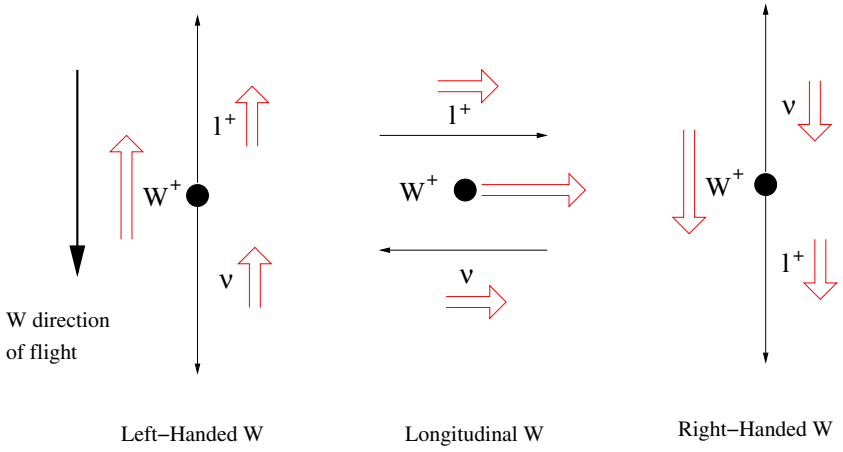

Fig. 2. Sketches of the different W^+ polarization modes in $t \to W^+b$ decay and resulting lepton directions. Simple (open) arrows denote particle direction of motion (spin). For W^-, left and right-handed components are inverted

direction, leading to a softer (harder) p_T spectrum with respect to the leptons from longitudinal W^+. The resulting angular lepton distributions are therefore very distinct for each W helicity state.

As it is necessary to know the weak isospin of the W spin analyzer, the charged lepton is the best choice since u-like jets can not be distinguished experimentally from d-like jets. Consequently, the W polarization is better measured in dileptonic and semileptonic $t\bar{t}$ channels through the distribution of the Ψ angle between the charged lepton direction in the W rest frame and the W direction in the top quark rest frame. The Ψ angular distribution is given by the following expression [6]:

$$\frac{1}{N}\frac{dN}{d\cos\Psi} = \frac{3}{2}\left[F_0\left(\frac{\sin\Psi}{\sqrt{2}}\right)^2 + F_L\left(\frac{1-\cos\Psi}{2}\right)^2 + F_R\left(\frac{1+\cos\Psi}{2}\right)^2\right] \quad (2)$$

Its SM expectation is shown in Fig. 3. It reflects the superposition of the three terms of (2), corresponding to the longitudinal $(\sin\Psi)^2$, the left-handed $(1-\cos\Psi)^2$ and the right-handed $(1+\cos\Psi)^2$ W helicity states. Each term is weighted by the fraction F_0, F_L or F_R given in (1).

Since the W and top rest frames are used in the Ψ angle measurement, it requires a complete event topology reconstruction. This is rather easy in the semileptonic $t\bar{t}$ channel, with only one neutrino in the final state and a high signal over background ratio (see Sect. 3.4.1). In the dileptonic channel[2], the event reconstruction is more challenging (see Sect. 3.4.2). Therefore, the Ψ angle is reconstructed in terms of the invariant mass of the lepton and the b-quark, M_{lb} [6]:

$$\cos\Psi \sim \frac{2M_{lb}^2}{M_t^2 - M_W^2} - 1 \quad (3)$$

which is valid in the zero b-mass limit, and where M_t and M_W are set to 175 GeV and 80.41 GeV, respectively. In this approach, the dependence on the b-jet energy scale and on the top mass uncertainty is high. On the contrary, these two dependences cancel at first order when measuring directly $\cos\Psi$. A study performed in the semileptonic channel shows a two times lower systematics on F_0, F_L and F_R using the $\cos\Psi$ observable compared to that obtained with M_{lb}^2.

[2] This is also the case at the Tevatron [19–22] and for single top analysis at LHC [16].

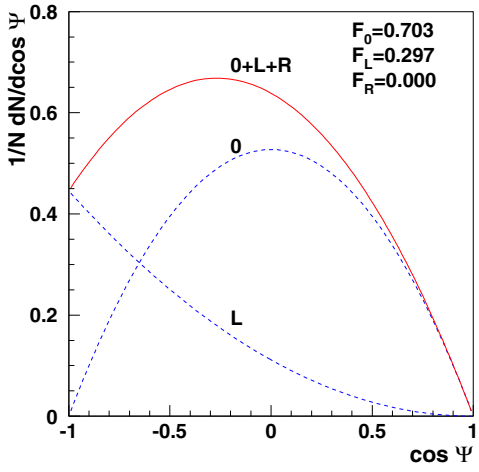

Fig. 3. Angular distribution of (2) in the SM. The predicted contributions from longitudinal (0) and left-handed (L) helicity states are shown separately with dashed lines. The right-handed contribution is null in the SM. The sum (0+L+R) is depicted with a full line

2.2 Top polarization observables

Similarly as for the W, the top polarization can be analyzed trough the angular distribution of its daughters. In this case, the spin analyzer, denoted by i, can be either a direct daughter (W, b) or a W decay product (l, ν, j_1 or j_2). The relevant angular distribution is [14]:

$$\frac{1}{N}\frac{dN}{d\cos\theta_i} = \frac{1}{2}(1 + S\alpha_i\cos\theta_i) \quad (4)$$

where S is the modulus of the top polarization and θ_i is the angle between the direction of particle i in the top quark rest frame and the direction of the top polarization. α_i is the spin analyzing power of this particle. It is the degree to

Table 1. SM spin analyzing power at LO and NLO of top quark daughters: b-jet, W^+, and W decay products : lepton (l^+), j_1, j_2 or the least energetic non b-jet in the top rest frame, called lej [24]. The top quark is spin up. Signs are reversed for a spin down or for an anti-quark

Particle	b-jet	W^+	l^+	j_1=$\bar{d}$-jet, $\bar{s}$-jet	j_2=u-jet, $\bar{c}$-jet	lej
α_i (LO)	-0.41	0.41	1	1	-0.31	0.51
α_i (NLO)	-0.39	0.39	0.998	0.93	-0.31	0.47

which its direction is correlated to the spin of the parent top quark. It has been computed at the next-to-leading order (NLO) since long for the lepton (l) [23] and more recently for the b quark, the W boson and the quarks from the W decay [24]. The theoretical values are given both at LO and NLO in Table 1 for a spin up top quark (signs are reversed for a spin down or for an anti-quark). Even if W and b are direct daughters of the top, their analyzing power is low due to the intrinsic polarization of the W which interferes destructively with the top one. Consequently, at LO, the difference $F_0 - F_L$ provides a measurement of α_W [25]. Charged leptons and down-type quarks, which are almost 100% correlated with the top spin direction, are optimal spin analyzers. But on the contrary to leptons, d and s-jets cannot be distinguished experimentally from u and c-jets. Therefore, the analyzing power of light jets is the average value $\alpha_{\rm jet} \sim (1 - 0.31)/2 = 0.35$. This can be improved by choosing the least energetic jet (lej) in the top rest frame, which is of d type in 61% of the case, resulting to $\alpha_i \sim 0.5$ [24].

Equation (4) can be directly used for top quarks produced lonely via the weak interaction, which are polarized ($S \sim 1$). This is not the case of the top quarks produced in $t\bar{t}$ pairs, which are not polarized [26]. However, the top and the anti-top spins are correlated, which can be easily understood. Close to the $t\bar{t}$ production threshold, the $t\bar{t}$ system produced by $q\bar{q}$ annihilation (gg fusion) is in a $^3S_1$ ($^1S_0$) state [5]. Therefore, in the first case, the top quarks tend to have their spins aligned while in the second case their spins tend to be opposite to each other. Away from threshold, this simple picture is modified due to the presence of angular momentum. In the absence of polarization, a direct measurement of the correlation at the level of the top quarks is obtained from observables of the form:

$$(\hat{\mathbf{a}} \cdot \mathbf{S}_t)(\hat{\mathbf{b}} \cdot \mathbf{S}_{\bar{t}}),\ (\mathbf{S}_t \cdot \mathbf{S}_{\bar{t}}) \tag{5}$$

where $\mathbf{S}_t$, $\mathbf{S}_{\bar{t}}$ are the spin operators of the top and anti-top, and $\hat{\mathbf{a}}$, $\hat{\mathbf{b}}$ are arbitrary directions ($|\hat{\mathbf{a}}| = |\hat{\mathbf{b}}| = 1$). A more familiar representation of the observables shown in (5) can be obtained from the relation:

$$\begin{aligned} A &= 4\langle(\hat{\mathbf{a}} \cdot \mathbf{S}_t)(\hat{\mathbf{b}} \cdot \mathbf{S}_{\bar{t}})\rangle \\ &= \frac{\sigma(t_\uparrow\bar{t}_\uparrow) + \sigma(t_\downarrow\bar{t}_\downarrow) - \sigma(t_\uparrow\bar{t}_\downarrow) - \sigma(t_\downarrow\bar{t}_\uparrow)}{\sigma(t_\uparrow\bar{t}_\uparrow) + \sigma(t_\downarrow\bar{t}_\downarrow) + \sigma(t_\uparrow\bar{t}_\downarrow) + \sigma(t_\downarrow\bar{t}_\uparrow)} \end{aligned} \tag{6}$$

where $\sigma(t_{\uparrow/\downarrow}\bar{t}_{\uparrow/\downarrow})$ denotes the cross section for the production of a top quark pair with spins up or down with respect to a quantization axis defined by $\hat{\mathbf{a}}$ in case of the top quark and $\hat{\mathbf{b}}$ in case of the anti-top quark. Note that rewriting the observable $(\mathbf{S}_t \cdot \mathbf{S}_{\bar{t}})$ using

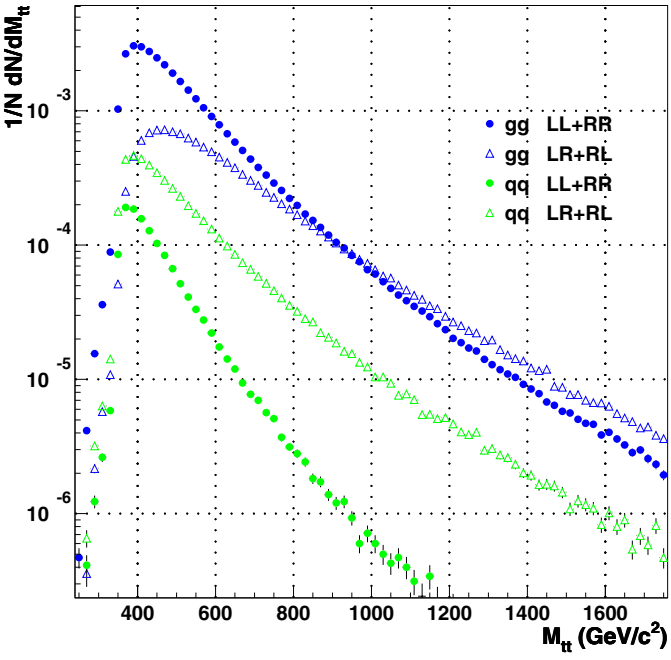

Fig. 4. Invariant mass distribution of the $t\bar{t}$ system with like (LL+RR) and unlike (LR+RL) helicities for the two possible production mechanisms (gg and $q\bar{q}$) [28]

$$A_D = (\mathbf{S}_t \cdot \mathbf{S}_{\bar{t}}) = \sum_i S_{ti} S_{\bar{t}i} = \sum_i \left(\hat{\mathbf{e}}^{(i)} \cdot \mathbf{S}_t\right)\left(\hat{\mathbf{e}}^{(i)} \cdot \mathbf{S}_{\bar{t}}\right) \tag{7}$$

where $\hat{\mathbf{e}}_k^{(i)} = \delta_{ik}$, the observable $(\mathbf{S}_t \cdot \mathbf{S}_{\bar{t}})$ can also be cast into the form shown in (6). Computation in the Standard Model gives favorably like-spin pairs ($A > 0$) when using the 'helicity' basis for the spin basis at LHC [15]. In this basis[3], the top (anti-top) spin quantization axis corresponds to the top (anti-top) direction of flight in the $t\bar{t}$ center of mass system, and the notation $\uparrow, \downarrow$ is replaced by L (Left) and R (Right). Figure 4 shows the invariant mass distribution of the $t\bar{t}$ system with like and unlike helicities for the two possible production mechanisms. As already explained, gg and $q\bar{q}$ processes contribute to the asymmetry with opposite signs ($A > 0$ for gg and $A < 0$ for $q\bar{q}$). The theoretical Standard Model value integrated over the whole LHC spectrum at LO is $A = 0.319$ and A_D=-0.217.

[3] Another basis was recently found to be more optimal, but more complicated to reconstruct [27].

At NLO these values become [29]:

$$\begin{cases} A = 0.326^{+0.003}_{-0.002}(\mu)^{+0.013}_{+0.001}(PDF), \\ A_D = -0.237^{+0.005}_{-0.007}(\mu)^{+0.000}_{-0.006}(PDF) \end{cases} \quad (8)$$

Systematic uncertainties come from factorization and renormalization scales ($\mu = \mu_F = \mu_R$) and from Parton Distribution Function (PDF). As A and A_D are defined as ratios between two cross sections, PDF, μ and α_S dependences cancel to a large extent. Moreover, NLO QCD corrections are small and thus theoretical uncertainties are well under control.

At LHC, it is possible to increase the asymmetry by applying an upper cut on the $t\bar{t}$ invariant mass $M_{t\bar{t}}$. As shown in Fig. 4, the asymmetry is maximal at low invariant masses for the gg contribution, which is by far dominant at the LHC, and is equal to 0 around $M_{t\bar{t}} = 900\,\text{GeV}$. Therefore, selecting low energetic top quarks with $M_{t\bar{t}} < 550\,\text{GeV}$ rejects only 30% of the events while A and A_D are enhanced by about 30% at LO:

$$\begin{cases} A = 0.422, \\ A_D = -0.290 \end{cases} \quad (9)$$

Similarly to (4) for top polarization, angular distributions can be used to probe the $t\bar{t}$ spin correlation, as:

– the double differential angular distribution of top and anti-top quark decay products [30]:

$$\frac{1}{N}\frac{d^2N}{d\cos\theta_1 d\cos\theta_2} = \frac{1}{4}(1 + B_1\cos\theta_1 + B_2\cos\theta_2 - C\cos\theta_1\cos\theta_2) \quad (10)$$

where θ_1 (θ_2) is the angle between the direction of the t ($\bar{t}$) spin analyzer in the t ($\bar{t}$) rest frame and the t ($\bar{t}$) direction in the $t\bar{t}$ center of mass system. These complicated angles are the direct consequence of the choice of the 'helicity' basis for measuring the asymmetry. As top and anti-top quarks are not polarized in this basis, $B_1 = B_2 = 0$. Figure 5 (top panel) illustrates this double angular distribution for the SM in the semileptonic channel.

– the opening angle distribution [29]:

$$\frac{1}{N}\frac{dN}{d\cos\Phi} = \frac{1}{2}(1 - D\cos\Phi) \quad (11)$$

where Φ is the angle between the direction of flight of the two spin analyzers, defined in the t and $\bar{t}$ rest frames respectively. Figure 5 (down panel) shows this opening angle distribution for the SM in the semileptonic channel.

In (10) and (11), C and D are the spin correlation observables. Before any phase-space cut, they can be easily measured using the following unbiased estimators [31]:

$$\begin{cases} C = -9 < \cos\theta_1\cos\theta_2 >, \\ D = -3 < \cos\Phi > \end{cases} \quad (12)$$

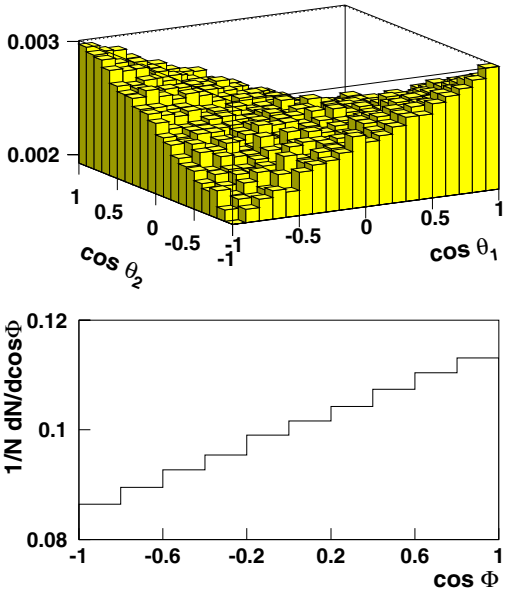

Fig. 5. Up, double differential angular distribution of (10). Down, opening angle distribution of (11). Both are shown at parton level with $M_{t\bar{t}} < 550\,\text{GeV}$

The production asymmetries A and A_D are then directly deduced by simply unfolding the decay contribution through the spin analyzing power of the daugther particles α_1 and α_2:

$$\begin{cases} A = \dfrac{C}{|\alpha_1\alpha_2|}, \\ A_D = \dfrac{D}{|\alpha_1\alpha_2|} \end{cases} \quad (13)$$

Since leptons are the most powerful spin analyzers ($\alpha = 1$), the dileptonic case is a priori the most promising. On the contrary, the all hadronic case is the most unfavorable, with a low spin analyzing power and a huge background. Several choices exist in the semileptonic channel for the spin analyzers on the hadronic side (W, b and lej) and experimentally the lej is the best choice [32]. In any case the semileptonic channel is more challenging compared to the dileptonic one because its spin analyzers are less powerful than the leptons. But on the contrary to the dileptonic channel, the number of events is 6 times larger and the event reconstruction is much easier (only one neutrino in the final state).

3 Event simulation, selection and reconstruction

This section describes the software tools used to generate and simulate signal and background events using a modeling of the ATLAS detector. Then the event selection and reconstruction is explained in both $t\bar{t}$ semileptonic and dileptonic channels.

3.1 Signal and background definition

General figures of $t\bar{t}$ pairs decay are: $Br(t \to Wb) \sim 1$, $Br(W \to l\nu_l) \sim 1/3$ with $l = e, \mu, \tau$ in equal probabilities and $Br(W \to q_1 q_2) \sim 2/3$ with $q_1(q_2) = u(d), c(s)$ in equal probabilities. With a NLO cross-section around 850 pb [33], 3.8 (0.9) millions of $t\bar{t}$ semileptonic (dileptonic) events will be produced with an integrated luminosity of $10\,\mathrm{fb}^{-1}$, corresponding to one LHC year at low luminosity. Among them, 2.5 (0.4) millions are signal events, defined as:

$$\begin{cases} t\bar{t} \to WbW\bar{b} \to l\nu b j_1 j_2 \bar{b}, \\ t\bar{t} \to WbW\bar{b} \to \bar{l}\nu b l \bar{\nu} \bar{b} \end{cases}$$

with $l = e, \mu$. The 1.3 (0.4) million events with at least one $l = \tau$ in the semileptonic (dileptonic) channel are considered as background. Non-$t\bar{t}$ background is composed of QCD background, from which mainly $b\bar{b}$ production is relevant for our study, and of electroweak backgrounds, which are W+jets, $Z(\to ll)$+jets, $Wb\bar{b}$, 2 vector bosons (ZZ, ZW, WW) and single top production.

3.2 Event generation

The Monte Carlo leading-order generator TopReX 4.05 [34] is used for the $t\bar{t}$ event generation. It includes the Standard Model LO $t\bar{t}$ spin correlation[4]. A top mass of 175 GeV is assumed and the structure function CTEQ5L [36] is used. The Q^2-scale ($p_T(t)^2$+M_t^2) used for α_S is the same as for the structure function. The proportion of gg and $q\bar{q}$ processes, which directly impacts the spin correlation (see Fig. 4), is 86%/14%. Partons are fragmented and hadronized using PYTHIA 6.2 [37], including initial and final state radiations, as well as multiple interactions, in agreement with CDF data extrapolated to LHC [38]. The b-fragmentation is performed using the Peterson parametrization with $\epsilon_b = -0.006$. TAUOLA and PHOTOS [39] are used to process the τ-decay and radiative corrections. All results correspond to one LHC year at low luminosity. For the systematics study, samples corresponding to three times (ten times) more statistics are generated for each source of uncertainties in the semileptonic (dileptonic) channel.

For what concerns the non-$t\bar{t}$ background generation in the semileptonic channel, PYTHIA is used, except for W+4 jets and $Wb\bar{b}$ which are treated with AlpGen [40] and AcerMC [41] generators, respectively. About $3 \cdot 10^{10}$ $W(\to l\nu)$+4 jets weighted events are generated with cuts on the four extra light jets: p_T >10 GeV, $|\eta| < 2.5$ and ΔR(jet-jet) >0.4[5]. Despite this huge effort, it only represents $1/63^{rd}$ of the statistics for one LHC year (380 000 events). For $b\bar{b}$ background, given the very high cross-section (∼500 μb) of the process, the cut $\sqrt{\hat{s}}$ >120 GeV is applied at the parton level. 750 million of events have been generated, corresponding to $1/8^{th}$ of the statistics for one year. Anyway, as this QCD background is very difficult to estimate, it should be extracted from the data. Except for W+4 jets and $b\bar{b}$, the statistics corresponding to one LHC year at low luminosity is simulated for each background without any cut at the parton level. In the dileptonic case, all backgrounds are simulated using PYTHIA 6.2, except for $Z/\gamma^* b\bar{b}$ that is generated with AcerMC.

[4] NLO spin correlation simulations are expected to be included in the future in MCatNLO [35] generator.

[5] $\Delta R = \sqrt{\Delta\phi^2 + \Delta\eta^2}$

3.3 Detector modeling

A simplified modeling of the ATLAS detector, ATLFAST 2.6.0 [42], is used. This essentially accounts for resolution smearing of objects accepted within the detector geometry, according to the expected performances [43]. Only settings of particular importance are recalled here:

- Isolation criteria only for lepton (electron and muon) consists in: *i*) asking $E_T < 10$ GeV in a pointing cone of 0.2 around the lepton and *ii*) requiring the nearest calorimeter cluster at $\Delta R > 0.4$.
- Jets are reconstructed with a cone algorithm, with a size $\Delta R = 0.4$. They are calibrated to obtain a correct jet energy scale [43].
- A 60% b-tagging efficiency is assumed, as well as a c-jet rejection of 10. For the other jets, the rejection is 100. This is a rather pessimistic assumption compared to the latest simulation results [44].

No trigger inefficiencies and no detailed acceptance (as crack between barrel and endcap) are included in this analysis. A 90% lepton and a 95% jet reconstruction efficiency are assumed.

3.4 Event selection and reconstruction

The heavy top mass makes the event topology at LHC outstanding: t and $\bar{t}$ are preferentially produced in the central region ($|\eta| < 2.5$), back to back in the transverse plane and are therefore naturally well separated.

3.4.1 Semileptonic $t\bar{t}$ events

Semileptonic signal events are characterized by one (and only one) isolated lepton, at least 4 jets of which 2 are b-jets, and missing energy. They are selected by requiring an isolated lepton from first and second level trigger. The offline kinematic cut on the lepton is directly given by the trigger threshold which is set to $\mathrm{p}_T > 20$ GeV at $10^{33}\,\mathrm{cm}^{-2}\,\mathrm{s}^{-1}$. Moreover, at least four jets with $\mathrm{p}_T > 30$ GeV are required, among which at least two are b-tagged. This p_T cut is a good compromise between a low combinatorial background and a good statistics. The 20 GeV cut on the missing transverse energy ($\mathrm{p}_T^{\mathrm{miss}}$) is standard for events with one neutrino and rejects almost no signal events. All these kinematic cuts are summarized in Table 2. Their resulting efficiency on signal events is 6.5%. The average p_T of the lepton and least energetic jet in the top rest frame (lej) are around 50 GeV.

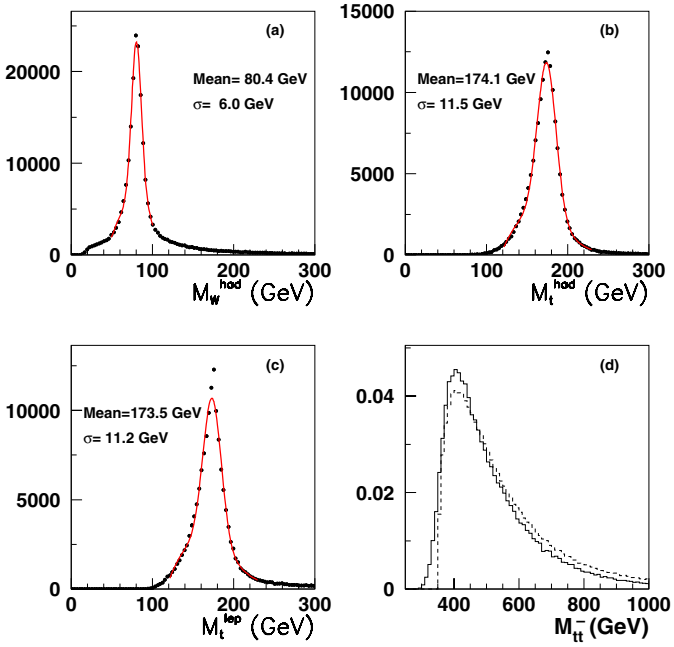

Fig. 6. a–c Reconstructed masses of W from hadronic side, top from hadronic and leptonic sides in the semileptonic channel. Lines correspond to Gaussian+third order polynomial fits, from which Mean and σ are extracted. **d** Normalized reconstructed mass distributions of the $t\bar{t}$ system are shown both in the semileptonic (full) and dileptonic (dashed) channels

After kinematic cuts, the full event topology is reconstructed. On the top hadronic decay side, the two non b-jets with M_{jj} closest to the known M_W [45] are selected. The di-jet invariant mass is shown in Fig. 6a, and the event is kept if the mass difference is lower than 20 GeV. Then, the b-jet with M_{jjb} closest to the known M_t [45] is chosen to reconstruct the hadronic top. The remaining b-jet is used for the leptonic top reconstruction, and for the 5% of events with more than two b-jets, the one closest to the lepton in ΔR is chosen. The missing transverse momentum is used to evaluate the neutrino p_T. Its longitudinal component, p_z, is determined by constraining $M_{l\nu}$ to M_W, keeping the solution with $M_{l\nu b}$ closest to M_t:

$$\left[E^l + \sqrt{(p_T^\nu)^2 + (p_z^\nu)^2}\right]^2 - (p_x^l + p_x^\nu)^2 - (p_y^l + p_y^\nu)^2 - (p_z^l + p_z^\nu)^2 = M_W^2 \qquad (14)$$

Table 2. Selection cuts in the semileptonic $t\bar{t}$ channel

Selection type	Variables	Cuts
Kinematic and acceptance	=1 isolated lepton	$p_T > 20$ GeV, $\|\eta\| < 2.5$
	≥ 4 jets	$p_T > 30$ GeV, $\|\eta\| < 2.5$
	b-tagged jets	≥ 2
	Missing energy (ν)	$p_T^{miss} > 20$ GeV
Reconstruction quality	$\|M_W^{had}\text{-}M_W\|$	< 20 GeV
	$\|M_t^{had}\text{-}M_t\|$	< 35 GeV
	$\|M_t^{lep}\text{-}M_t\|$	< 35 GeV

Table 3. Number of events in the semileptonic $t\bar{t}$ channel (signal and background) for one LHC year at low luminosity, 10 fb^{-1}, before and after selection cuts

	Initial number of events ($\times 10^6$)	Number of selected events
Signal ($t\bar{t}$ semileptonic)	2.5	85000
$t\bar{t}$ background		
$t\bar{t} \to \tau + X$	1.3	6200
$t\bar{t} \to$ all had	3.7	70
Non-$t\bar{t}$ background		
$W(\to l\nu)$+4 jets	24	[400,1000]
$b\bar{b}$ ($\sqrt{\hat{s}} > 120$ GeV)	6000	200
$Z(\to ll)$+jets	49	12
ZZ, WW, ZW	1.1	5
$W(\to l\nu)b\bar{b}$	0.7	3
single top	1.0	350

For 25% of the events, there is no solution since p_T^{miss} overestimates p_T^ν. In these cases, p_T^ν is decreased step by step by 1% until a solution is reached [46].

Figures 6b,c show reconstructed top masses. Results are comparable with those of the top mass study [47]. Quality cuts are then applied on top and anti-top reconstructed masses ($|M_t^{had} - M_t| < 35$ GeV and $|M_t^{lep} - M_t| < 35$ GeV) to reject badly reconstructed events. At this stage, 3.3% of the signal events are kept, corresponding to 85000 signal events for one LHC year at low luminosity. Table 2 lists all the selection cuts.

After selection criteria are applied, the background is composed for more than 80% of $t\bar{t} \to \tau + X$ events, as shown in Table 3. The amplitude and shape of this $t\bar{t}$ background should be easily under control. The remaining non-$t\bar{t}$ background is dominated by $W(\to l\nu)$+4 jets, $b\bar{b}$ and single top events. In the first two cases, since only a few tens of events subsist after all cuts, Poisson statistics is used to give an estimate of the expected number of events. Given its very low contribution to the overall background, the non-$t\bar{t}$ background will be neglected in the rest of the analysis. In total, about 7000 background events are expected for one LHC year at low luminosity, giving a signal over background ratio of 12.

For the top spin study, to enhance the correlation, a further cut, $M_{t\bar{t}} < 550$ GeV, is applied on the $t\bar{t}$ reconstructed mass (Sect. 2.2), whose distribution is shown in Fig. 6d. The total efficiency becomes 2.3%, corresponding to 60000 signal events for one LHC year at low luminosity.

3.4.2 Dileptonic $t\bar{t}$ events

Dileptonic events are characterized by two (and only two) opposite charged isolated leptons, at least two jets of which two are b-jets, and missing energy. They are selected by requiring two leptons from first and second level trigger. The offline p_T cut on opposite sign leptons is conservatively set to 20 GeV, well above the trigger thresholds which are

Table 4. Selection cuts in the dileptonic $t\bar{t}$ channel

Selection type	Variables	Cuts
	=2 isolated leptons	$p_T > 20\,\text{GeV}$, $\|\eta\| < 2.5$
Kinematic and	≥ 2 jets	$p_T > 20\,\text{GeV}$, $\|\eta\| < 2.5$
acceptance	b-tagged jets	$= 2$
	Missing energy (ν)	$p_T^{\text{miss}} > 40\,\text{GeV}$
Reconstruction quality	$M_{t\bar{t}}$	$< 550\,\text{GeV}$

lower or equal to 15 GeV for two leptons. Moreover, two b-tagged jets with $p_T > 20\,\text{GeV}$ are required. The 40 GeV cut on p_T^{miss} is standard for events with two neutrinos. Table 4 shows the selection cuts in the dileptonic channel. Their total efficiency on signal events is 6.5%.

After kinematic cuts, the event topology is reconstructed using the algorithm developed in [48]. The aim of the reconstruction is to obtain the unknown momenta of neutrino and anti-neutrino and the association between the two b-jets and the b and $\bar{b}$ quarks. To solve the set of six non-linear equations coming from the momenta and energy conservation, the known M_t and M_W are assumed. The set of equations can have up to four solutions for each combination of the association b-jets to b and $\bar{b}$ quarks. The choice of the solution is based on the computation of weights from known distribution of transversal momenta of t, $\bar{t}$ and ν, $\bar{\nu}$. The reconstruction efficiency of this algorithm[6] is 80% with the correct solution found in 65% of the cases. Most of the dilution comes from the wrong b assignation. After cuts and reconstruction, 5.3% of the signal events are kept, corresponding to 21000 signal events for one LHC year at low luminosity. The background is then composed for 90% of $t\bar{t} \to \tau + X$ events, as shown in Table 5. In total, 4000 background events are expected for one LHC year at low luminosity, giving a signal over background ratio of 5, more than two times lower than in the semileptonic channel.

Table 5. Number of events in the dileptonic $t\bar{t}$ channel (signal and background) for one LHC year at low luminosity, $10\,\text{fb}^{-1}$, before and after selection cuts

	Number of events ($\times 10^6$)	Number of selected events
Signal ($t\bar{t}$ dileptonic)	0.4	21000
$t\bar{t}$ background		
$t\bar{t} \to \tau + l$	0.5	3700
$t\bar{t} \to l + jet$	3.8	40
Non-$t\bar{t}$ background		
$b\bar{b}$ ($\hat{p_T} > 20\,\text{GeV}$)	30000	<200
Z+jets, W+jets, ZZ, WW, ZW	4500	<100
$Z/\gamma^*(\to ll)b\bar{b}$	1.7	250
single top	1.0	7

[6] Fraction of selected events for which a solution of the kinematical equations exists.

As in the semileptonic case, a cut on the $t\bar{t}$ reconstructed mass, $M_{t\bar{t}} < 550\,\text{GeV}$, whose distribution is shown in Fig. 6d, dashed lines, is applied to enhance the spin correlation. In this case, the total efficiency becomes 3.5%, corresponding to 15000 signal events for one LHC year at low luminosity.

4 Sensitivity to W boson polarization in $t\bar{t}$ events

In this section the method to extract the W polarization observables is explained (Sect. 4.1), the complete systematics study is presented (Sect. 4.2) and results combining dileptonic and semileptonic channels are given (Sect. 4.3). Finally, using these results, the sensitivity to tWb anomalous couplings is discussed (Sect. 4.4).

4.1 Measurement method

As charged leptons from longitudinal W have a harder p_T spectrum than those from left-handed W, they are more likely to pass the trigger threshold and offline selection requirements. More generally, the reconstructed $\cos\Psi$ angular distribution is distorted by all the acceptance and reconstruction effects compared to the parton level one, as shown in Fig. 7. This leads to a bias in the measurement, which is more pronounced as the cut on the lepton p_T increases. To correct for it, a weight is applied on an event by event basis, allowing to recover, as much as possible, the original shape. The weighting function is obtained from the ratio between the two normalized distributions of Fig. 7 (i.e. after selection cuts and at parton level) for semileptonic and dileptonic events. In both channels, this ratio, shown in Fig. 8, is fitted by a third order polynomial function to extract a smooth correction. The fit is restricted to the region $-0.9 < \cos\Psi < 0.9$, which is the most extended region where the correction is varying slowly. The correction functions, computed on an independent data sample, are then applied event by event on the analysis samples.

The final distribution after event selection and correction is shown in Fig. 9 for semileptonic and dileptonic events, corresponding to one year at low luminosity, $10\,\text{fb}^{-1}$. The W polarization is extracted from a fit in the restricted region with the (2) function and the constraint $F_0 + F_L + F_R = 1$. The results for F_0, F_L and F_R are compatible with their SM expectations. The statistical errors

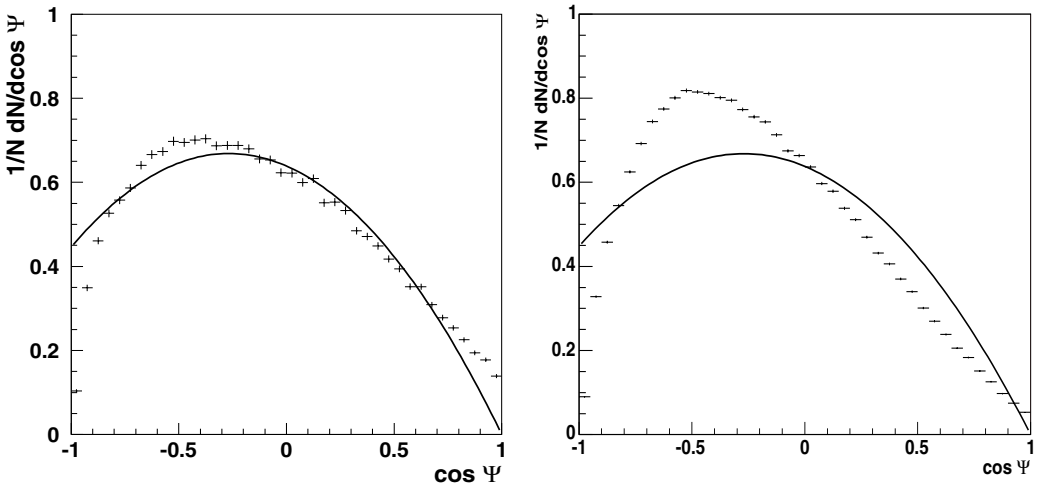

Fig. 7. Normalized $\cos\Psi$ distribution after selection cuts (histogram) for semileptonic (left) and dileptonic (right) $t\bar{t}$ events. For comparison, the SM parton level distribution (Fig. 3) is superimposed (full line)

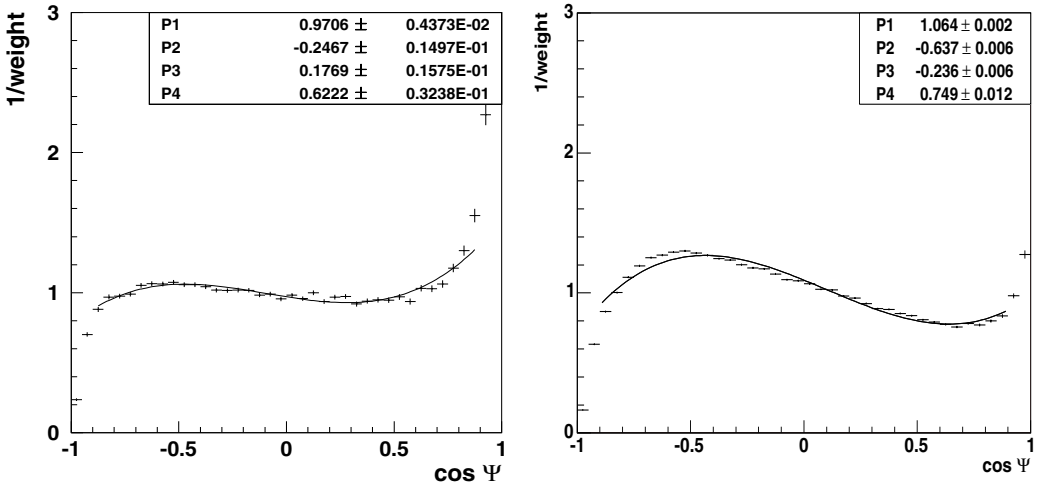

Fig. 8. Ratio between the two normalized distributions of $\cos\Psi$ shown in Fig. 7, i.e. after selection cuts and at parton level, for semileptonic (left) and dileptonic (right) $t\bar{t}$ events. The full line is the result of a third order polynomial fit in the range $-0.9 < \cos\Psi < 0.9$

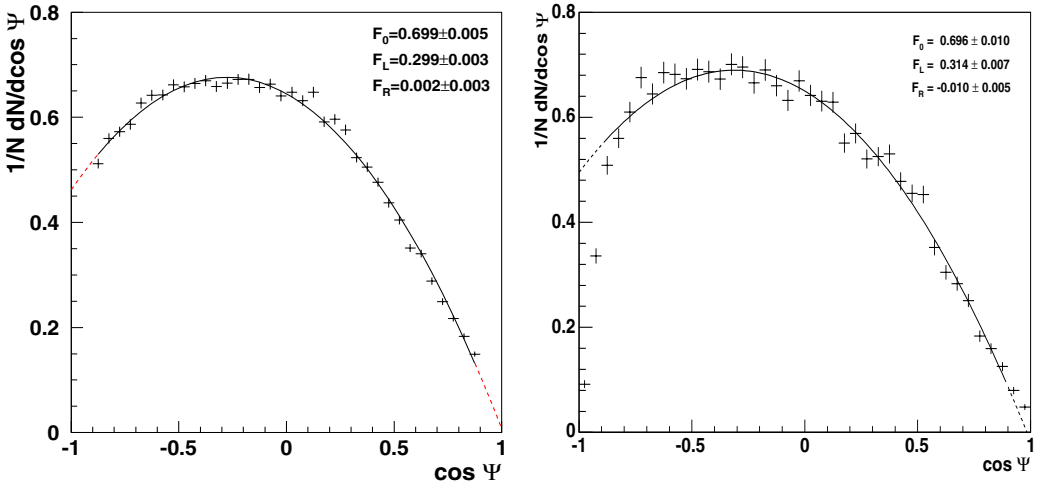

Fig. 9. Normalized $\cos\Psi$ distribution after selection cuts and correction for semileptonic (left) and dileptonic (right) $t\bar{t}$ events after one year at low luminosity, $10\,\mathrm{fb}^{-1}$. The full line is the result of a fit with function of (2) in the range $-0.9 < \cos\Psi < 0.9$, with $F_0 + F_L + F_R = 1$. The dashed line represents the continuation of the function outside the fit region

are 0.005 for F_0 and 0.003 for F_L and F_R in the semileptonic case and increase to 0.010, 0.007 and 0.005 in the dileptonic case. The correlation between the parameters for the couples (F_0,F_L), (F_0,F_R) and (F_L,F_R) are -0.9, -0.8 and 0.4.

The systematic uncertainty induced by the weighting method has been estimated by varying the number of bins (from 40 to 25), the fit limits (from [-0.9;0.9] to [-0.8;0.8]) and the polynomial order (from P3 to P5 and P7). All variations are below the statistical error. Therefore, the total uncertainty of the method is estimated to be smaller than the statistical error.

The corrections functions of Fig. 8 are extracted with a Standard Model scenario, assuming a pure V-A top decay vertex. In case of deviation from the SM, the kinematic distributions, such as lepton p_T or angles can be affected.

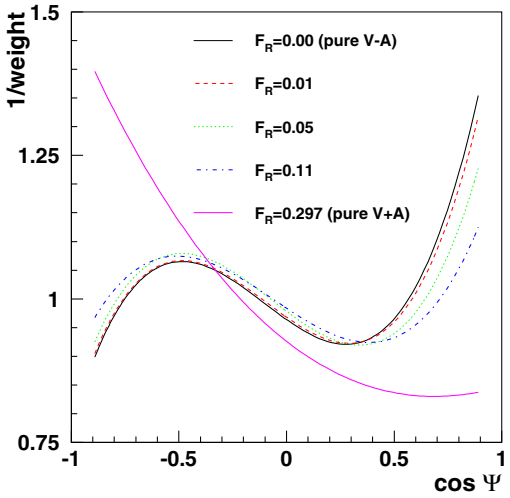

Fig. 10. Correction functions for different F_R input values in the semileptonic channel. The case $F_R = 0$ corresponds to the SM, and the case $F_R = 0.297$ corresponds to a pure V+A model. The SM function (pure V-A) is the one of Fig. 8

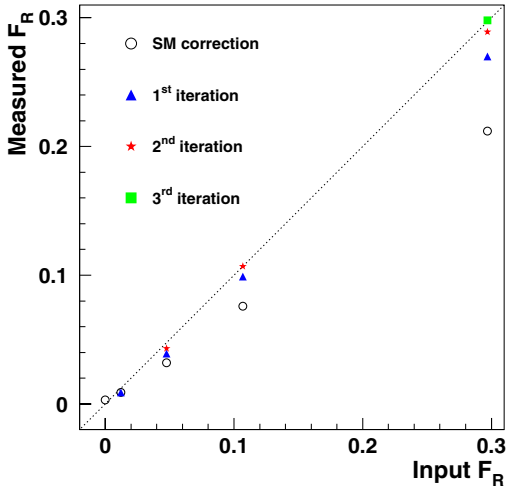

Fig. 11. F_R extracted from the fit as a function of F_R input values. The open circles correspond to the measurement using the SM correction. Full triangles, stars and squares correspond to the first, second and third iteration, respectively (see text). The dotted line is $y = x$

This is for example the case if a V+A component is present. In such a scenario, the fraction of longitudinal W bosons will be unchanged, but a right component F_R, whose lepton spectrum is harder (see Sect. 2.1) will appear. As a consequence, the correction function will be changed. This is illustrated in Fig. 10 for different F_R input values. In each case, the statistics of one LHC year of semileptonic events has been generated with AlpGen. Applying the SM correction function to these samples will therefore not correct completely for the bias induced by the selection cuts. Figure 11 shows the fraction F_R extracted from the fit[7] as a function of the F_R input value after applying the SM correction function (open circles). The measurement is clearly biased. To overcome this problem we proceed iteratively. The SM correction function is first used. Then, in case of deviation of F_R from zero, a new correction function is calculated with this new F_R component, and applied. The process converges after a few iterations, as shown in Fig. 11.

4.2 Systematic uncertainties

This section presents a detailed study of the systematic uncertainties related to the W polarization measurement.

4.2.1 Systematic uncertainties at generation level

In this subsection, five main sources of systematic uncertainties are considered:

- *Q-scale*: The uncertainty related to the Q-scale at parton generation is estimated by comparing samples generated with TopReX and AlpGen using default Q^2-scale: $p_T(t)^2 + \mathrm{M}_t^2$ and M_t^2. In both cases, the same hadronization scheme (PYTHIA) is used.
- *Structure function*: The impact of the structure function is estimated by the maximum difference between the measurements obtained with the standard parton density function (CTEQ5L) and three other ones, CTEQ6L [49], MRST2002 [50] and GRV98 [51]. It is conservatively estimated to be independent of the above Q-scale uncertainty.
- *ISR, FSR*: The presence of initial state radiations (ISR) from incoming partons and especially final state radiations (FSR) can affect the Ψ angle reconstruction since it impacts the top quark reconstruction. To estimate the effect due to ISR, the difference between the measurements obtained with ISR switched on (usual data set) and off is computed. The same approach is used for FSR. The level of knowledge of ISR and FSR is around 10%, reflecting the uncertainty on α_s. Therefore, as a more conservative estimate, the systematics uncertainties have been taken to be 20% of the corresponding differences. It should be noted that more sophisticated methods exist to make this evaluation [52].
- *b-fragmentation*: The b-quark fragmentation is performed according to the Peterson parametrization[8], with one free parameter ϵ_b. The default value is set to $\epsilon_b = -0.006$. It has been changed to a more recent LEP value ($\epsilon_b = -0.0035$ [54]), and the differences on the results are taken as systematic uncertainties, which are conservative estimates.
- *Hadronization scheme*: The angular distributions of jets and leptons may be influenced by the hadronization scheme. Generating partons with AcerMC then processing the hadronization with PYTHIA or HERWIG [55] leads to different W polarization measurements. For this study the default settings of PYTHIA and HER-

[7] In this case, F_0 is fixed to its SM value and the only fitted parameter is F_R.

[8] It has to be noticed that recent measurements can not be well fitted with the Peterson parametrization [53].

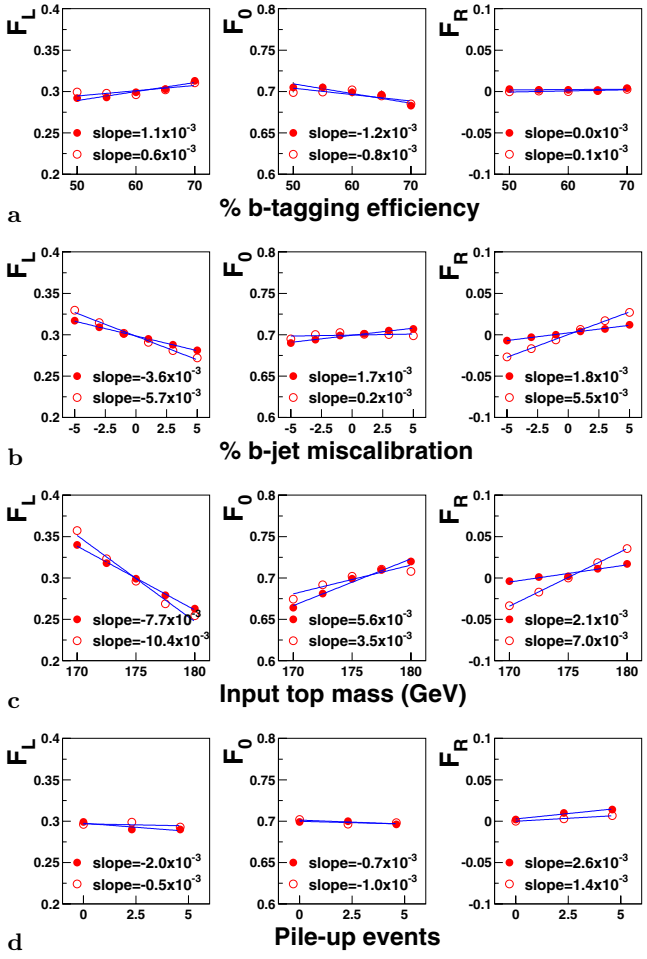

Fig. 12a–d. Measured F_L (left), F_0 (middle) and F_R (right) in the semileptonic (black circles) and dileptonic (open circles) $t\bar{t}$ channels as a function of different parameters, see text for more details. Linear fits are superimposed in each case, and the corresponding slope is indicated

WIG, tuned on various experiments data, were used, leading to a conservative systematic estimate.

4.2.2 Systematic uncertainties at reconstruction level

In this subsection, three main sources of systematic uncertainties are considered:

- *b-tagging*: The impact of the b-tagging efficiency is studied by increasing it from 50% to 70% by steps of 5%, according to a parametrization coming from full simulation [44]. Increasing the b-tagging efficiency degrades the c-jets and light jets rejection factors. As an example, going from 55% to 60% decreases them respectively by 30% and 80%. Figure 12a shows F_L, F_0 and F_R measurements as a function of the b-tagging efficiency. Small and smooth dependences are observed. The related error is computed with a realistic ±5% uncertainty on the b-tagging efficiency.
- *Jet miscalibration*: The impact of the knowledge of the absolute b-jet energy scale is estimated by miscalibrating the reconstructed b-jet energy. Results are shown in Fig. 12b, for a miscalibration between ±5% by steps of 2%. The behaviors can be easily understood: a positive miscalibration overestimates the invariant mass of the lepton and the b-quark, M_{lb} and therefore $\cos\Psi$, (3). This bias the polarization toward higher values (F_L decreases and F_R increases). The corresponding systematic is computed with a realistic ±3% uncertainty on the b-jet energy scale. Similarly, the effect of ±1% light jet energy miscalibration has been studied and has no impact on the results.
- *Input top mass*: The SM W polarization has a small dependence on the top mass, with an increase (decrease) of F_0 (F_L) by 0.002 per GeV, (1). Moreover, a 175 GeV top mass value is assumed in the event reconstruction, which can impact the $\cos\Psi$ measurement if the real top mass is different. Therefore, different samples of events were generated with a top mass between 170 and 180 GeV by steps of 2.5 GeV. Results are shown in Fig. 12c. As for the case of a positive b-jet miscalibration, a high top mass increases M_{lb}, and therefore bias the polarization toward higher values. The related systematics are -0.008 (-0.010) per GeV on F_L, 0.006 (0.003) on F_0 and 0.002 (0.007) on F_R in the semileptonic (dileptonic) channel. The final uncertainty is computed assuming $\Delta M_{\rm top}$=2 GeV, which should be reached at Tevatron run II [56].

4.2.3 Other sources of systematic uncertainties

- *Background*: As shown in Sect. 3.4, the only sizable background comes from $t\bar{t} \to \tau + X$ events, and is well under control. A large variation of this background level by ±10% has a negligeable impact on the results when considering the semileptonic channel because of the high signal over background ratio. In the dileptonic channel, this results in an uncertainty of 0.004 on F_L, 0.003 on F_0 and 0.001 on F_R.
- *Pile-up*: Extra jet activity may influence the reconstruction and therefore impact on W polarization measurement. Different samples were generated (with the PYTHIA settings MSTP(131)=1 and MSTP(132)=4), adding 2.3 or 4.6 pile-up events according to the Poisson law. These numbers are expected for a luminosity of $10^{33}\,{\rm cm}^{-2}{\rm s}^{-1}$ and $2\times10^{33}\,{\rm cm}^{-2}{\rm s}^{-1}$, respectively. Figure 12d shows that the impact is small, even if no jet recalibration is applied. Other jet activity uncertainties due to the underlying event modelization are therefore expected to be negligible.

4.2.4 Systematics summary

All systematic uncertainties are listed in Table 6 and illustrated in Figs. 13 and 14 for the semileptonic and dileptonic channels, respectively. Generation and reconstruction sources contribute roughly in the same proportion to the total error. The dominant generation contributions come from the FSR knowledge, the hadronization scheme and the Q-scale. while the reconstruction systematics are

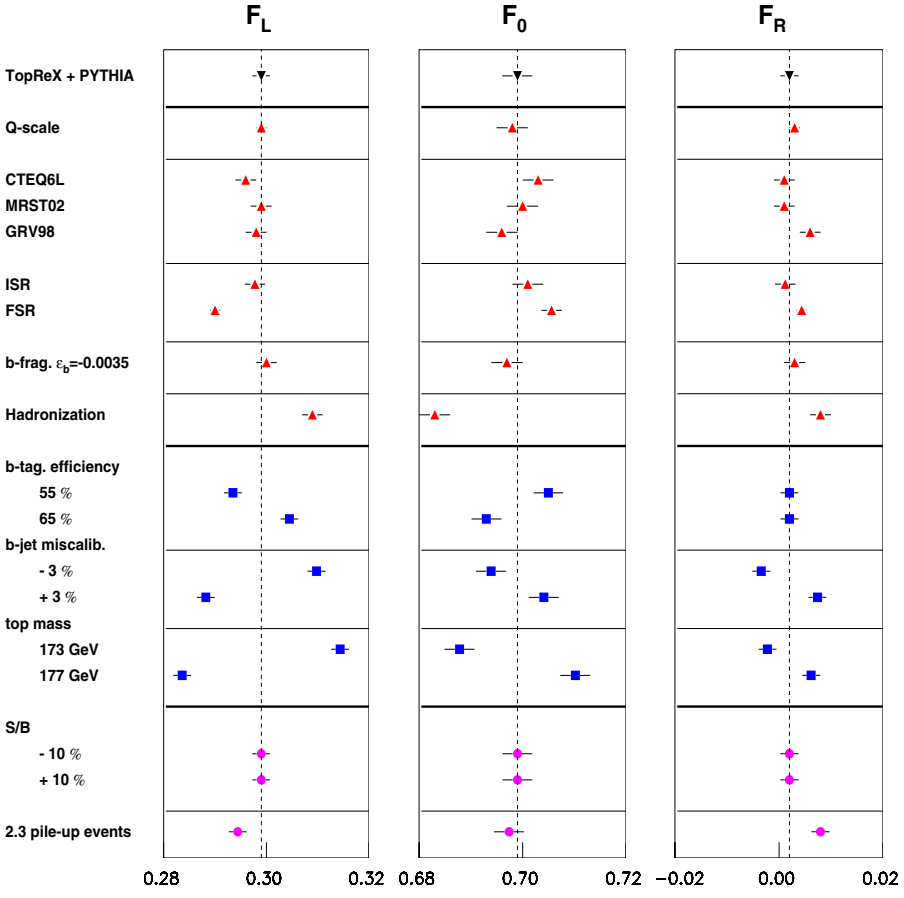

Fig. 13. Systematic uncertainties on F_L, F_0 and F_R in the semileptonic $t\bar{t}$ channel

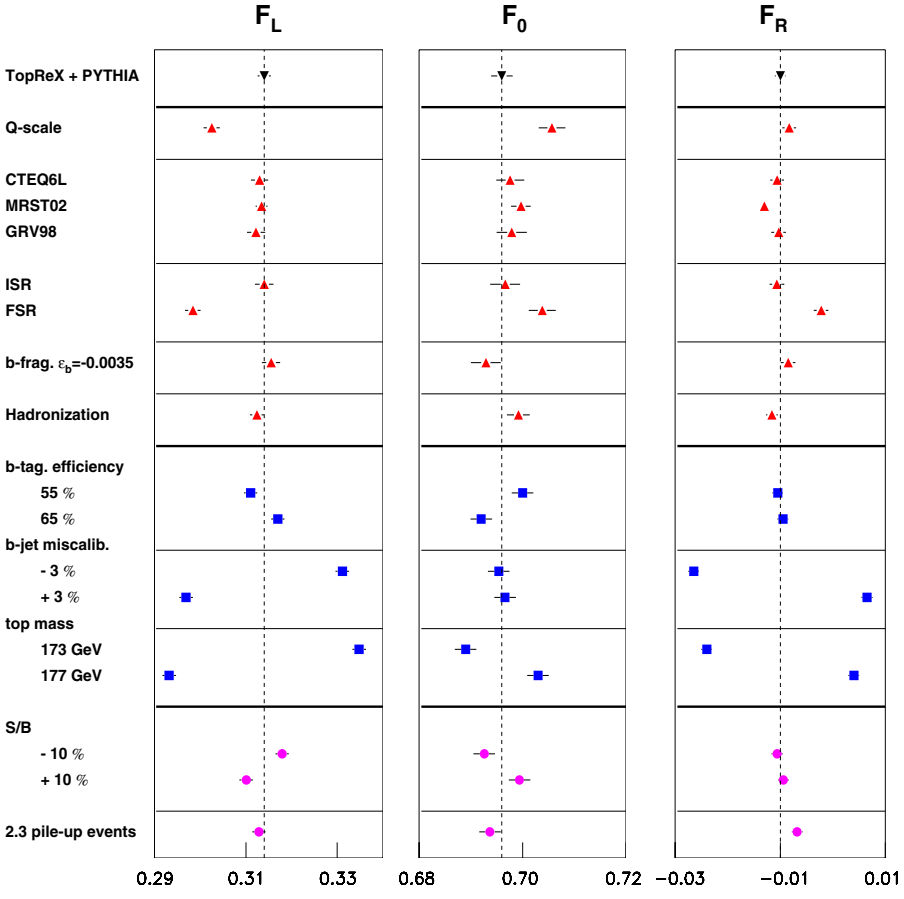

Fig. 14. Systematic uncertainties on F_L, F_0 and F_R in the dileptonic $t\bar{t}$ channel

Table 6. Summary of systematics on F_L, F_0 and F_R in the semileptonic and dileptonic $t\bar{t}$ channels

Source of uncertainty	Semileptonic channel			Dileptonic channel		
	F_L	F_0	F_R	F_L	F_0	F_R
Generation						
Q-scale	0.000	0.001	0.001	0.011	0.010	0.002
Structure function	0.003	0.003	0.004	0.002	0.004	0.003
ISR	0.001	0.002	0.001	0.000	0.001	0.001
FSR	0.009	0.007	0.002	0.016	0.008	0.008
b-fragmentation	0.001	0.002	0.001	0.002	0.003	0.002
Hadronization scheme	0.010	0.016	0.006	0.002	0.003	0.002
Reconstruction						
b-tagging (5%)	0.006	0.006	0.000	0.003	0.003	0.001
b-jet miscalibration (3%)	0.011	0.005	0.005	0.017	0.001	0.017
Input top mass (2 GeV)	0.015	0.011	0.004	0.021	0.007	0.014
Others						
S/B scale (10%)	0.000	0.000	0.000	0.004	0.003	0.001
Pile-up (2.3 events)	0.005	0.002	0.006	0.001	0.002	0.003
TOTAL	0.024	0.023	0.012	0.034	0.016	0.024

Table 7. Standard Model results for W polarization components after one LHC year of data taking ($10^{33}\,\mathrm{cm^{-2}s^{-1}}$, $10\,\mathrm{fb^{-1}}$) in semileptonic and dileptonic $t\bar{t}$ channels. A combination of both results is presented in the last column

	Semileptonic ($\pm$stat$\pm$syst)	Dileptonic ($\pm$stat$\pm$syst)	Semilep+Dilep
F_L	$0.299 \pm 0.003 \pm 0.024$	$0.314 \pm 0.007 \pm 0.034$	$0.303 \pm 0.003 \pm 0.024$
F_0	$0.699 \pm 0.005 \pm 0.023$	$0.696 \pm 0.010 \pm 0.016$	$0.697 \pm 0.004 \pm 0.015$
F_R	$0.002 \pm 0.003 \pm 0.012$	$-0.010 \pm 0.005 \pm 0.024$	$0.000 \pm 0.003 \pm 0.012$

dominated by the b-jet miscalibration and the top mass uncertainty.

4.3 Results

Table 7 presents the expected Standard Model results for the W polarization measurement in $t\bar{t}$ semileptonic and dileptonic channels after one LHC year at low luminosity ($10^{33}\,\mathrm{cm^{-2}s^{-1}}$, $10\,\mathrm{fb^{-1}}$). The sensitivity is driven by the systematic uncertainties, which largely dominates the statistical ones. F_L and F_R parameters are more precisely measured in the semileptonic channel, while the accuracy on F_0 is slightly better in the dileptonic one. Combining the results of both channel studies, assuming a pessimistic 100% correlation of systematic errors, lead to the results shown in Table 7, rightmost column. The only improvement of the combination concerns F_0 on which the absolute error is estimated to be 0.016. It is worth to notice that F_R, which is expected to be zero in the SM, is the most precisely measured with an accuracy of 0.012.

This result is 3 times better than the statistical error foreseen with single top events ($\sim$ 0.03 on F_R with $10\,\mathrm{fb^{-1}}$) [16]. It is also roughly 3 to 5 times better than the Tevatron run II statistical expectations with $2\,\mathrm{fb^{-1}}$ ($\sim$ 0.03 on F_R [57] and $\sim$ 0.09 on F_0 [58]). CDF and D0 published first measurements of the W polarization in $t\bar{t}$ pairs based on Run I data [19–21]. For example, CDF results are $F_0 = 0.91 \pm 0.37(\mathrm{stat}) \pm 0.13(\mathrm{syst})$ and $F_R = 0.11 \pm 0.15$. They are largely limited by statistical errors[9]. Preliminary studies started at Run II [22], but statistical errors will remain large, even with the total integrated luminosity of $2\,\mathrm{fb^{-1}}$ [59].

The results of Table 7 were obtained assuming realistic uncertainties of 3% on the b-jet energy scale and 2 GeV on the top mass. More pessimistic assumptions (5% and 3 GeV) lead to an increase of the total systematic errors on F_L, F_0 and F_R to 0.031, 0.018 and 0.013. On the contrary, more optimistic assumptions (1% and 1 GeV) lead to 0.018, 0.014 and 0.009. In all cases, the absolute error on F_R remains in the range 0.009–0.013 and that on F_0 in the range 0.015–0.018. The assumptions on systematic uncertainties have therefore a small impact, assessing the robustness of the results.

All above results were obtained with a $10^{33}\,\mathrm{cm^{-2}s^{-1}}$ luminosity. The luminosity may be $2 \cdot 10^{33}\,\mathrm{cm^{-2}s^{-1}}$ at the LHC start. In this case, two scenarios are considered in ATLAS for the single electron trigger: increase of the single electron p_T cut at the trigger level from 20 to 25 GeV

[9] A few tens of both dileptonic and semileptonic $t\bar{t}$ events, with an integrated luminosity of $109\,\mathrm{pb^{-1}}$ ($125\,\mathrm{pb^{-1}}$) for CDF (D0).

(scenario 1), or even to 30 GeV (scenario 2). The complete study has been redone in the semileptonic channel for both scenarios, assuming the same hypothesis for each source of systematic uncertainty presented in Fig. 13. The number of events will be multiplied by 1.8 (1.6) for scenario 1 (scenario 2), while systematic errors remain almost unchanged. Consequently, the same precision will be achieved on the W polarization measurement. At high luminosity, $10^{34}\,\mathrm{cm}^{-2}\mathrm{s}^{-1}$, a possible improvement can be to consider leptonic final states with J/ψ, in a similar way as what is performed for the top mass measurement [47].

The forward-backward asymmetry, A_{FB}, based on the angle between the charged lepton and the b-jet in the W rest frame, is often discussed in literature [60]. It can be expressed in terms of F_L and F_R [17]:

$$A_{FB} = \frac{3}{4}\,(F_L - F_R\,) \qquad (15)$$

Taking the correlation between F_L and F_R into account, the following measurement on A_{FB} can be extracted from the previous results:

$$A_{FB} = 0.227 \pm 0.003(\mathrm{stat}) \pm 0.016(\mathrm{syst}) \qquad (16)$$

Nevertheless, it does not provide any more information than the separate measurements of the ratios F_L and F_R.

4.4 Sensitivity to new physics

As already stated in the introduction, the search for anomalous (i.e. non Standard Model) interactions is one of the main motivations for top quark physics. The measurement of the W polarization provides a direct test of our understanding of the tWb vertex, responsible for practically all top quark decays in the Standard Model (SM). The deviations from the SM expectations induced by new physics contributions have been calculated in the framework of a few models [61–64]. However, because of the great diversity of models beyond the SM (Supersymmetry, dynamical electroweak symmetry breaking models, extra dimensions,...), it is also useful to study these possible new interactions in a model independent approach [7,65–67]. The unknown dynamics can be parametrized with couplings representing the strength of effective interactions, through the following Lagrangian [6]:

$$\mathcal{L} = \frac{g}{\sqrt{2}} W_\mu^- \bar{b}\gamma^\mu (f_1^L P_L + f_1^R P_R) t - \frac{g}{\sqrt{2}\Lambda} \partial_\nu W_\mu^- \bar{b}\sigma^{\mu\nu}(f_2^L P_L + f_2^R P_R) t + h.c. \qquad (17)$$

where $P_{R/L} = \frac{1}{2}(1 \pm \gamma_5)$, $\sigma^{\mu\nu} = \frac{i}{2}[\gamma^\mu, \gamma^\nu]$, g is the electroweak coupling constant and Λ is the energy scale to which the new physics becomes apparent (in the following, Λ =M$_W$ is set to keep the notation used in the literature). f_1^L and f_1^R are vector-like couplings, whereas f_2^L and f_2^R are tensor-like couplings. This is the most general CP-conserving Lagrangian keeping only the leading (mass dimension 4, first term) and the next-to-leading (mass dimension 5, second term) effective operators in the low energy expansion. In the SM, the values of the couplings at tree level are $f_1^L = V_{tb} = 1$, $f_1^R = f_2^L = f_2^R = 0$.

It will first be shown how the measurement of the W polarization in top decay can probe these anomalous couplings (Sect. 4.4.1) and then a review of their existing direct and indirect experimental limits will be given (Sect. 4.4.2).

4.4.1 Probe of tWb anomalous couplings

The contributions of f_1^L, f_1^R, f_2^L and f_2^R anomalous couplings to each fraction of helicity state, F_L, F_0 and F_R, have been calculated at LO [6,68] and at NLO [60], NLO effects being small. A deviation of f_1^L from 1 has not been considered in the following, as the W helicity is not sensitive to it. This can be easily understood, as f_1^L is proportional to V_{tb}, which can not be directly measured with $t\bar{t}$ pairs but only with single top quarks.

In the following, an independent deviation of each anomalous coupling, f_1^R, f_2^L and f_2^R, is assumed. Figure 15 shows the variation of F_L, F_0 and F_R with these couplings. F_L and F_R depend quadratically on f_1^R, whereas F_0 remains unchanged (full lines). Similarly, the three fractions of helicity states are sensitive to f_2^L in a quadratic way (dashed lines). In these two cases, the sign of the coupling can not be determined and the sensitivity will be lowered by the quadratic behavior. The last case is the most interesting (dash-dotted lines): F_0 and F_L depend almost linearly on f_2^R with a slope=0.7 [69], while F_R is unchanged. Thus the sign of f_2^R can be determined: $F_0 > F_0^{SM}$ and $F_L < F_L^{SM}$ ($F_0 < F_0^{SM}$ and $F_L > F_L^{SM}$) signs the presence of negative (positive) anomalous coupling f_2^R. The sensitivity is also higher than for f_1^R and f_2^L. The precision to which F_L, F_0 and F_R can be measured (Table 7) sets the sensitivity to each anomalous coupling. It is represented by grey bands in Fig. 15. F_R is the most sensitive observable to probe f_1^R and f_2^L , whereas F_0 is better for f_2^R.

Figure 16 (full lines) shows the overall sensitivity (statistics+systematics) to each anomalous coupling that can be expected from the W polarization measurement with $t\bar{t}$ pairs at LHC. Dashed lines represent the statistical sensitivity only[10]. The corresponding 2σ limits (statistics+systematics) are given in Table 8. The best sensitivity is obtained on f_2^R due to the presence of the large linear dependence. It is of the order of the deviations expected by models like the Minimal Supersymmetric Standard Model (MSSM) or the Topcolor assisted Technicolor model (TC2) [68].

[10] A recent study at NLO on forward-backward asymmetry A_{FB} in $t\bar{t}$ pairs [60] indicates a 3σ statistical sensitivity with $100\,\mathrm{fb}^{-1}$ on $f_1^R \sim 0.06$, $f_2^L \sim 0.03$ and $f_2^R \sim 0.003$. This is in good agreement with our 3σ statistical sensitivity on $f_1^R \sim 0.17$, $f_2^L \sim 0.08$ and $f_2^R \sim 0.012$ obtained with $10\,\mathrm{fb}^{-1}$ only.

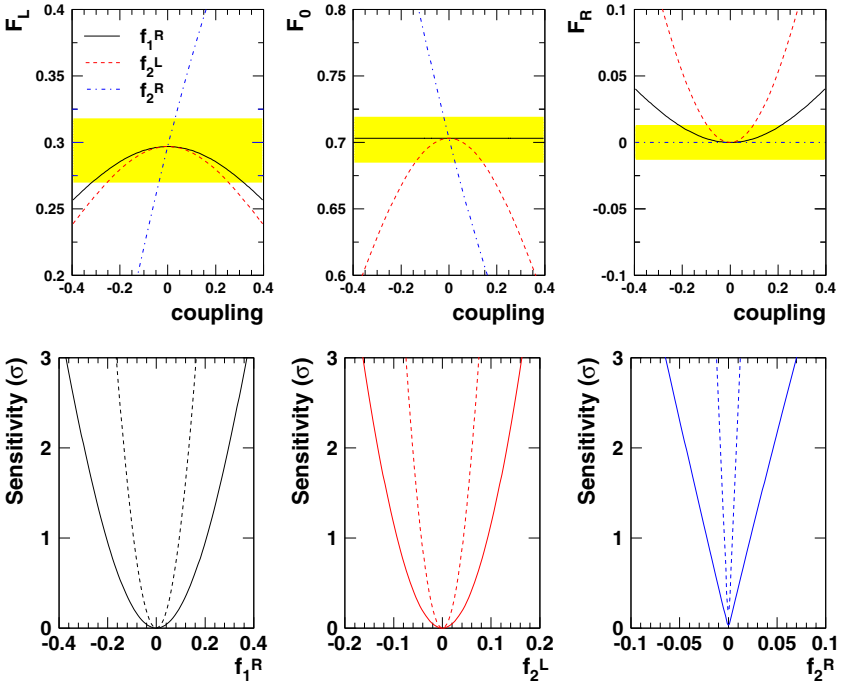

Fig. 15. F_0, F_L and F_R dependence on the anomalous couplings f_1^R (full lines), f_2^L (dashed lines) and f_2^R (dash-dotted lines). $f_1^L = 1$ is assumed. The expected 1σ uncertainties on F_0, F_L and F_R measured in $t\bar{t}$ pairs after one LHC year at low luminosity (Table 7) are indicated with grey bands

Fig. 16. Sensitivity in σ to the anomalous couplings f_1^R, f_2^L and f_2^R extracted from the W polarization measurement in $t\bar{t}$ pairs after one LHC year at low luminosity ($10\,\mathrm{fb}^{-1}$). Full lines indicate the overall (statistics+systematics) sensitivity, while dashed lines represent the statistical sensitivity only

Table 8. 2σ limits on anomalous couplings f_1^R, f_1^L and f_2^R. At LO, in the SM, these couplings are equal to zero. The first line presents our results extracted from the W polarization measurement in $t\bar{t}$ pairs after one LHC year at low luminosity ($10\,\mathrm{fb}^{-1}$). Expected limits at the Tevatron and with single top at LHC are shown in the next two lines. Current indirect limits from B-factories and LEP data are presented in the last two lines

	f_1^R	f_2^L	f_2^R
$t\bar{t}$, LHC ($10\ \mathrm{fb}^{-1}$) (Stat.+ Syst.)	0.30	0.13	0.04
$t\bar{t}$, Tevatron ($2\ \mathrm{fb}^{-1}$) (Stat. only)	0.5	0.3	0.3
single top, LHC ($100\ \mathrm{fb}^{-1}$) (Stat.+ 5% Syst.)	0.06	0.07	0.13
$b \to s\gamma, sl^+l^-$, B-factories (indirect)	0.004	0.005	0.4
Z decay, LEP (indirect)	–	–	0.1

4.4.2 Comparison with existing limits

The only existing direct limits on the tWb anomalous couplings can be placed from Tevatron W polarization measurements in $t\bar{t}$ pairs, which are limited by the low statistics. As an example, the run I result $F_R < 0.18$ at 95% C.L. [19] translates in $f_1^R < 0.8$. From run II expectations, statistical sensitivities to $f_1^R \sim 0.5$ and $f_2^{L,R} \sim 0.3$ [68] at 95% C.L can be achieved. The single top, which has not been experimentally observed so far, can provide further constraints on the tWb anomalous couplings from its production rate and kinematic distributions. At LHC, the expected 2σ limits are $-0.052 < f_2^L < 0.097$ and $-0.12 < f_2^R < 0.13$ [70] assuming a 5% systematic uncertainty, and a statistical sensitivity to $f_1^R \sim 0.06$ [71] with $100\,\mathrm{fb}^{-1}$, one LHC year at high luminosity. However, all these studies do not include any detector effect and detailed evaluation of systematic uncertainties. The related limits are summarized in Table 8 for each coupling.

Indirect limits on the tWb anomalous couplings have already been derived from precision measurements. The $b \to s\gamma$ and $b \to sl^+l^-$ decays proceed via an electroweak radiative penguin process [72]. As they include a tWb vertex, an anomalous coupling will result in a change of the branching ratios. The related limits on anomalous couplings are stringent: as an example, f_1^R has to be less than 0.004 [73] at 95% C.L. As the tWb coupling appears also in loop in Z decays, electroweak measurements from LEP/SLC give other indirect limits, mainly competitive on f_2^R. All these limits are presented for each coupling in the last two lines of Table 8. However, they are indirect, SM-dependent, and scenarios can be envisaged where other contributions lead to cancellations that invalidate these bounds.

To conclude, it is worth to notice that our expected sensitivity to the right-handed tensor-like coupling f_2^R is a factor 2–3 better than the best limit. In any case, the W polarization measurement in $t\bar{t}$ pairs and the single top studies at LHC will be complementary to determine the structure of the tWb vertex as precisely as possible.

5 Sensitivity to top quark polarization in $t\bar{t}$ events

As demonstrated in the previous section, the W polarization measurement provides a direct probe of the top decay mechanism. Using the same events, it is also possible to test the $t\bar{t}$ production by measuring the top spin asymmetries,

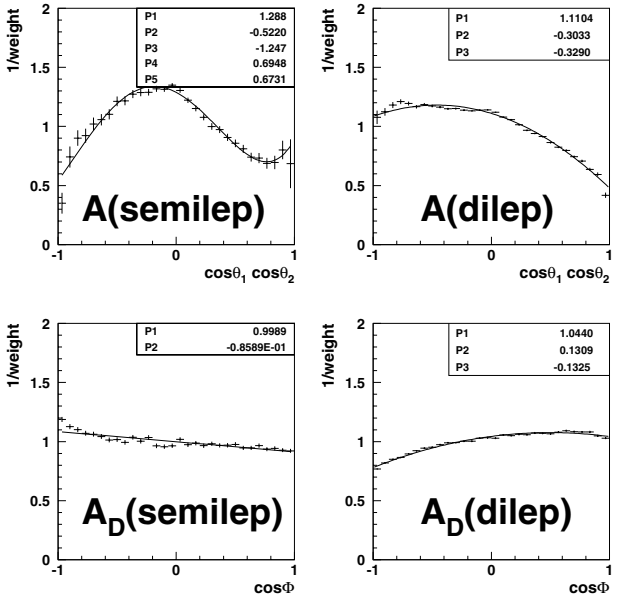

Fig. 17. Ratio between the distributions of $\cos\theta_1 \cos\theta_2$ (top) and $\cos\Phi$ (bottom) after selection cuts and at parton level for semileptonic (left) and dileptonic (right) $t\bar{t}$ events. The full lines are the results of polynomial fits

A and A_D. Similarly as for W polarization, we will explain the method used to extract these asymmetries (Sect. 5.1), present a complete study of systematic uncertainties in both semileptonic and dileptonic $t\bar{t}$ channels (Sect. 5.2), give the results combining both channels (Sect. 5.3), and finally discuss the related sensitivity to physics beyond the Standard Model (Sect. 5.4).

5.1 Measurement method

Similarly to the W polarization analysis (Sect. 4), selection cuts distort the parton level angular distributions. Therefore, expressions given in (12) are no longer unbiased estimators of the spin correlation observables. To correct for this bias, a weight is applied on an event by event basis, allowing to get back, as much as possible, the original asymmetry. One weight is applied per spin correlation observable (A and A_D) and per channel (semileptonic and dileptonic). The weighting functions are computed by fitting the selection efficiency in $\cos\theta_1 \cos\theta_2$ ($\cos\Phi$) bins for A (A_D). This is shown in Fig. 17, with a mean weight set to 1, which is the equivalent of Fig. 8 in the W polarization analysis. The four ratios are fitted by a polynomial function to extract smooth corrections. The A corrections have a wider range with respect to the A_D ones, proving that A_D is less affected by selection cuts. The correction functions, computed on an independent data sample, are then applied event by event on the analysis samples.

The correction functions are extracted with a Standard Model scenario. In case of deviation from the SM, the kinematic distributions can be affected, and the correction functions will be changed. This is illustrated in Fig. 18 (left plots) for different A (top) and A_D (bottom) input values

Table 9. Summary of systematics on A and A_D in the semileptonic and dileptonic $t\bar{t}$ channels

Source of uncertainty	Semileptonic channel		Dileptonic channel	
	A	A_D	A	A_D
Generation				
Q-scale	0.029	0.006	0.011	0.003
Structure function	0.033	0.012	0.008	0.005
ISR	0.002	0.001	0.001	0.001
FSR	0.023	0.016	0.005	0.000
b-fragmentation	0.031	0.018	0.007	0.004
Hadronization scheme	0.006	0.008	0.005	0.003
Reconstruction				
b-tagging (5%)	0.016	0.011	0.001	0.001
b-jet miscalibration (3%)	0.045	0.012	0.013	0.003
light-jet miscalibration (1%)	0.009	0.000	0.000	0.000
Input top mass (2 GeV)	0.028	0.013	0.009	0.001
Others				
S/B scale (10%)	0.000	0.000	0.003	0.004
Pile-up (2.3 events)	0.001	0.005	0.004	0.003
TOTAL	0.081	0.036	0.024	0.010

in the dileptonic channel[11]. For this purpose, different mixtures of events with/without spin correlation effects have been generated. Applying the SM correction function to these samples will therefore not correct completely for the bias induced by the selection cuts. Figure 18 (right plots) shows with open circles the measured asymmetries A (top) and A_D (bottom) as a function of their input values after applying the SM correction function. The measurement is clearly biased. As for Fig. 11 in the W polarization measurement, we proceed iteratively to overcome this problem. The SM correction function is first used. Then, in case of deviation from SM expectations a new correction function is calculated with this new asymmetry, and applied. The process converges after a few iterations, as seen in Fig. 18.

5.2 Systematic uncertainties

The same sources of systematic uncertainties as for the W polarization study (Sect. 4.2) are considered: five related to the generation (Q-scale, structure function, ISR-FSR, b-fragmentation and hadronization scheme), three to the reconstruction (b-tagging, b-jet miscalibration, input top mass), the background normalization and the pile-up influence. In the semileptonic channel, the light jet miscalibration is also taken into account as the least energetic jet in the top rest frame is used as spin analyzer. A particular attention was paid to the proportion of gg and $q\bar{q}$ processes involved in the $t\bar{t}$ pair production, which directly impacts

[11] This channel has been chosen to illustrate the method, as the bias due to the event reconstruction is more pronounced than in the semileptonic channel.

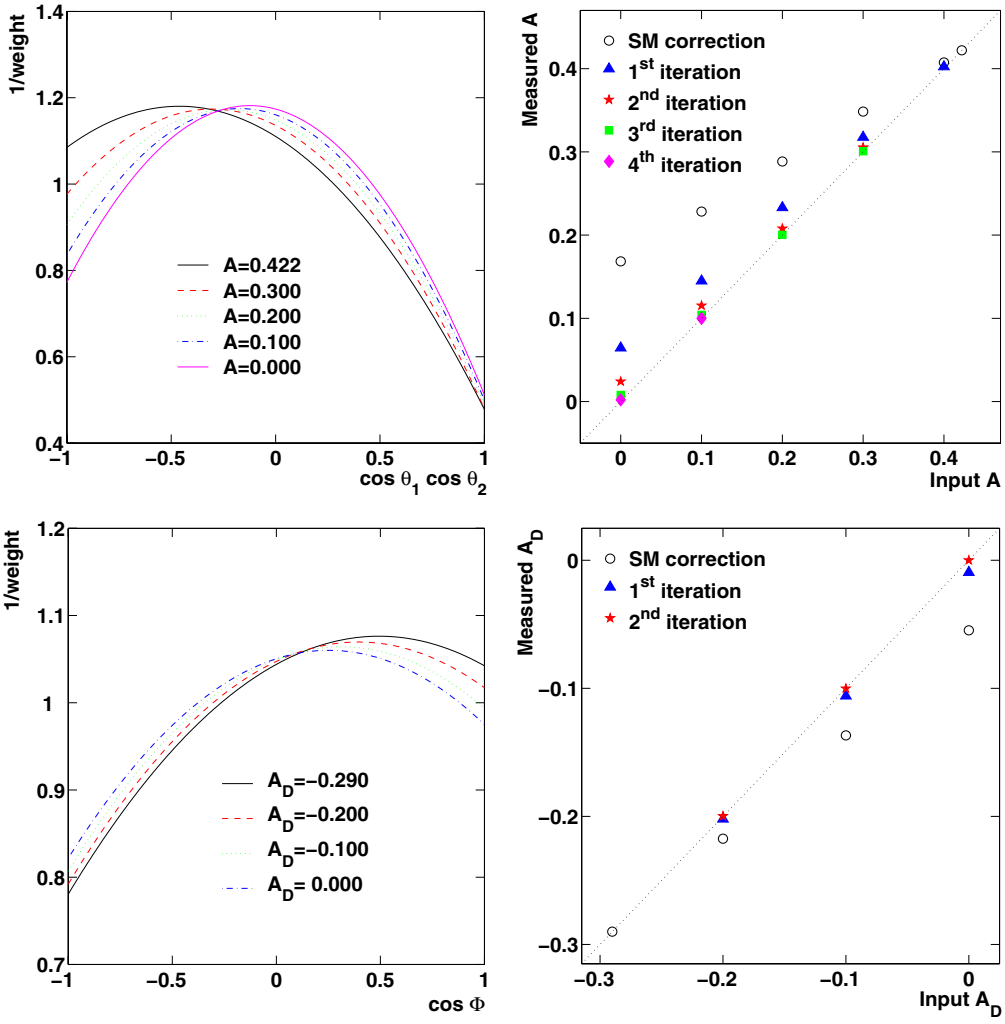

Fig. 18. Left: Correction functions for different A (top) and A_D (bottom) input values in the dileptonic channel. The case $A = 0.422$ and $A_D = -0.290$ corresponds to the SM functions of Fig. 17. Right: A (top) and A_D (bottom) after selection cuts and correction as a function of their input values. The open circles correspond to the measurement using the SM correction. Full triangles, stars, squares and diamonds correspond to the first, second, third and fourth iteration, respectively (see text). The dotted line is $y = x$

the spin correlation (see Fig. 4). To study separately this effect, samples with different proportions of $gg/q\bar{q}$ have been generated from 82%/18% to 90%/10% by steps of 2%. Small and smooth dependences are observed with a slope of 0.006 (0.004) per % of $gg/q\bar{q}$ variation for A (A_D).

The results obtained on A and A_D for different b-tagging efficiencies, b-jet miscalibrations, top masses and pile-up levels are detailed in Fig. 19. Linear behaviors are observed in both channels. All systematic uncertainties are listed in Table 9 and illustrated in Fig. 20. Generation and reconstruction sources contribute roughly in the same proportion to the total error. The dominant generation contributions come from the Q-scale, the structure function and the b-fragmentation, while the reconstruction systematics are dominated by the b-jet miscalibration and the top mass uncertainty. The total systematic error for A is 2.5 times higher than for A_D. This is because the angles are computed in the $t\bar{t}$ rest frame, more difficult to reconstruct than the top and anti-top rest frames separately. The lower systematics in the dileptonic channel are explained by the choice of two ideal spin analyzers (charged leptons).

5.3 Results

Table 10 presents the expected Standard Model results for A and A_D after one LHC year at low luminosity ($10^{33}\,\mathrm{cm}^{-2}\mathrm{s}^{-1}$, $10\,\mathrm{fb}^{-1}$). In the semileptonic channel, the sensitivity is driven by the systematic uncertainties, which largely dominates the statistical ones, while both errors are comparable in the dileptonic channel. Combining the results of both channel studies, assuming a pessimistic 100% correlation of systematic errors, lead to the results shown in Table 10, rightmost column. They allow to observe and measure the Standard Model spin correlation with a 4% precision.

Table 10. Standard Model results for spin correlation observables after one LHC year of data taking ($10^{33}\,\mathrm{cm^{-2}s^{-1}}$, $10\,\mathrm{fb^{-1}}$) in semileptonic and dileptonic $t\bar{t}$ channels. A combination of both results is presented in the last column

	Semileptonic (±stat±syst)	Dileptonic (±stat±syst)	Semilep+Dilep
A	$0.422 \pm 0.020 \pm 0.081$	$0.404 \pm 0.020 \pm 0.024$	$0.406 \pm 0.014 \pm 0.023$
A_D	$-0.288 \pm 0.012 \pm 0.036$	$-0.290 \pm 0.011 \pm 0.010$	$-0.290 \pm 0.008 \pm 0.010$

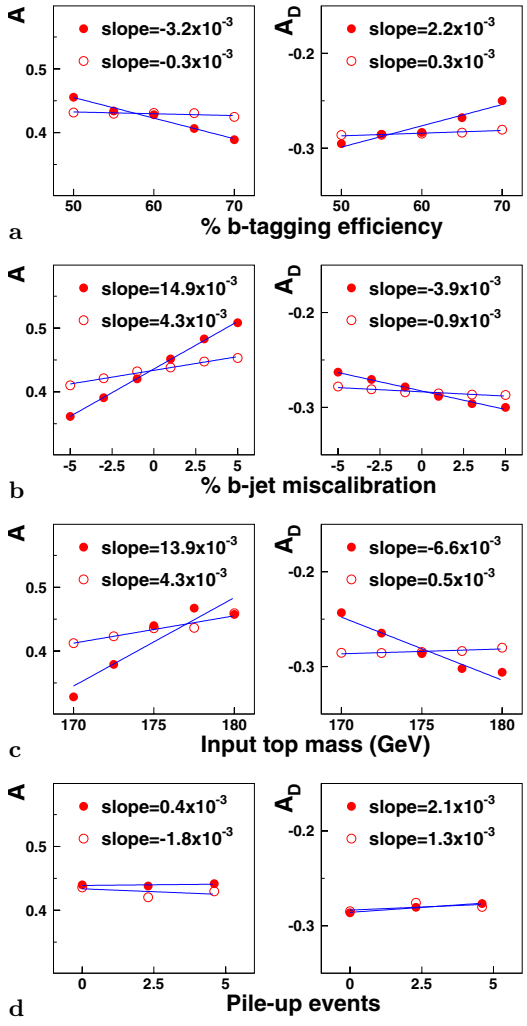

Fig. 19a–d. Measured A (left) and A_D (right) in the semileptonic (black circles) and dileptonic (open circles) $t\bar{t}$ channels as a function of different parameters, see text for more details. Linear fits are superimposed in each case, and the corresponding slope is indicated

This result can be compared with the 40% precision expected from Tevatron run II with $2\,\mathrm{fb^{-1}}$, neglecting the systematics. Experimentally, the $t\bar{t}$ spin correlation has never been observed. The D0 experiment sets a lower limit on A with 6 dilepton events from run I ($110\,\mathrm{pb^{-1}}$) [74]. This limit, $A > -0.25$ at 68% confidence level, can not be compared to the LHC values because the dominant production process at Tevatron is $q\bar{q} \to t\bar{t}$, and the Standard Model prediction is $A = 0.88$.

The results of Table 10 were obtained assuming realistic uncertainties of 3% on the b-jet energy scale and 2 GeV on the top mass. More pessimistic assumptions (5% and 3 GeV) lead to an increase of the total systematic errors on A and A_D to 0.030 and 0.011. On the contrary, more optimistic assumptions (1% and 1 GeV) lead to 0.015 and 0.009. In all cases, A_D remains in the range 4%-5%. The assumptions on systematic uncertainties have therefore a small impact, assessing the robustness of this result.

All above results were obtained with a $10^{33}\,\mathrm{cm^{-2}s^{-1}}$ luminosity. As already discussed in Sect. 4.3, the luminosity may be $2 \cdot 10^{33}\,\mathrm{cm^{-2}s^{-1}}$ at the LHC start and modify the p_T electron cut at the trigger level. The complete study has been redone in the semileptonic channel for the two foreseen scenarios, assuming the same hypothesis for each source of systematic uncertainty presented in Fig. 20. The number of events will be multiplied by 1.9 (1.8) for scenario 1 (scenario 2), while systematic errors remain unchanged. Consequently, the same sensitivity will be achieved for A and A_D measurements.

5.4 Sensitivity to new physics

As already stated in the introduction, a $t\bar{t}$ spin correlation observation would check that the top quark decays indeed as a quasi-free quark, i.e. in particular before hadronization can take place which could dilute the spin information. A measurement of the expected Standard Model spin correlation would test the top properties, with a left-handed coupling and a 1/2 spin. On one hand, this would allow to set an upper limit on its lifetime, directly linked to Cabibbo-Kobayashi-Maskawa matrix elements [75]. On the other hand, this would offer a unique opportunity to study a "bare" quark, free from long distance effects of QCD such as hadronization and confinement.

Therefore, a possible deviation of $t\bar{t}$ spin correlation from the SM prediction will be a hint of new physics. Its measurement can be used to probe the presence of new interactions. For example, $gt\bar{t}$ anomalous couplings, linked to chromoelectric [8] and chromomagnetic [9] dipole moments which naturally arise in dynamical electroweak symmetry breaking models such as technicolor or topcolor, can affect the resultant $t\bar{t}$ spin correlation [76]. This is also the case in the presence of either a new heavy resonance in the $t\bar{t}$ production, such as a spin 0 neutral Higgs boson [12] ($gg \to H \to t\bar{t}$), or spin 2 Kaluza-Klein (KK) gravitons [13]. As an example, in theories with large extra dimensions [77], the s-channel mediated by graviton KK modes gives rise to characteristic spin configurations and angular distributions for outgoing particles, which reflect

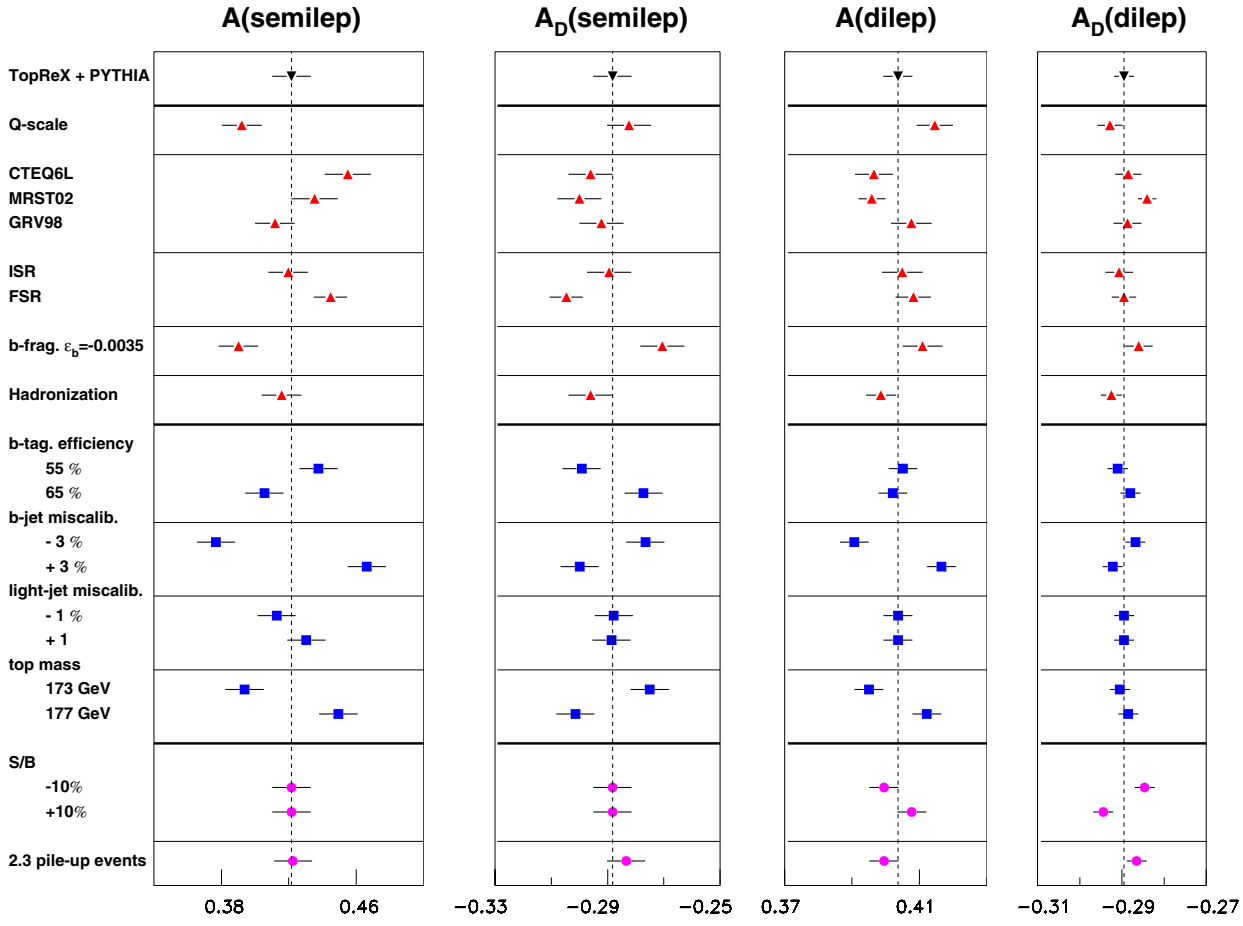

Fig. 20. Systematic uncertainties on A and A_D in the semileptonic and dileptonic $t\bar{t}$ channels

the spin-2 nature of the intermediate KK gravitons. With the sensitivity quoted in the previous section, a 5σ deviation from the SM $t\bar{t}$ spin correlation can be observed if the fundamental scale of the extra dimensional theory is below 1.5 TeV.

New interactions in the decay can also affect the $t\bar{t}$ spin correlation. As an example [15], if a sufficiently light charged Higgs boson exists, such as in supersymmetric models, the decay $t \to H^+b$ can compete with the SM decay mode $t \to W^+b$. As the charged Higgs decay to electrons and muons is largely suppressed, the deviation on the W-polarization measurement can be small. Contrarily, for m_{H^+} <150 GeV and at small $\tan\beta$ (< 2), the decay in two jets is favored, affecting the spin correlation in the semileptonic channel. As a result, with m_{H^+} ∼80 GeV, a 5σ deviation from the SM $t\bar{t}$ spin correlation can be observed if the branching ratio for top into charged Higgs plus b-quark is larger than 25%.

6 Conclusions

Because of its high mass, close to the electroweak symmetry breaking scale, the top quark is an ideal place to search for physics beyond the Standard Model. W polarization in top decay and top spin observables reflect in detail the interactions involved in top quark production and decay. Moreover, they can directly be inferred from the angular distributions of their respective decay products. Therefore, they give a good opportunity for precise tests of these interactions and are sensitive probes of new physics. Their precise measurements will be possible at the start of the LHC data taking, thanks to the very large sample of top events that will be accumulated. They will be complementary to V_{tb} and cross section measurements, as NLO QCD corrections and theoretical errors are much smaller, of the order of 1%.

The ATLAS capability to measure the W polarization components F_0, F_L and F_R (for longitudinal, left-handed and right-handed helicity fractions) and $t\bar{t}$ spin asymmetries (A, A_D) has been studied in the complementary semileptonic and dileptonic $t\bar{t}$ channels. The results of both channel studies have been combined. Leading-order Monte Carlo generators were used as well as a fast simulation of the detector. The clean signature of semileptonic $t\bar{t}$ events, a high statistics (around 100 000 signal events after selection and reconstruction in one year at low luminosity, 10 fb^{-1}) and a high signal over background ratio (more than 10) are the attractive features of this channel. In the dileptonic channel, the event topology reconstruction is complicated by the presence of two neutrinos in the final state, but feasible, the correct solution being found

in 65% of the events. Even if the statistics and the signal over background ratio are lower than in the semileptonic channel, it is an attractive channel for the top spin asymmetry measurement, because the two charged leptons of the final state are the most powerful top spin analyzers.

In both channels, selection cuts bias the measurements. A weighting method was set up to correct for it, and its robustness assessed. The sensitivity of the measurements is driven by the systematic uncertainties, which already dominates the statistical ones after one year at low luminosity. The main contributions to the total uncertainty come from the Q-scale, the hadronization scheme, the FSR knowledge, the b-jet energy scale and the top mass. After one LHC year, the Standard Model parameter F_0 can be measured with a 2% accuracy and F_R with a 1% precision, comparable to the expected precision on the top mass. Using the same selected events, the Standard Model top spin asymmetry can be measured with a precision around 4% with $10\,\mathrm{fb}^{-1}$. These results are robust against other hypothesis for systematic uncertainties and trigger scenarios.

The sensitivity to physics beyond the Standard Model can be deduced from the above results. This has been studied in a model independent approach on the decay side by introducing three tWb anomalous couplings, f_1^R, f_2^L and f_2^R, which parametrize new physics. The best sensitivity, a 2σ limit of 0.04, is obtained on f_2^R, which is better than indirect limits and expectations from other measurements. Finally, the sensitivity of the top spin measurement to new interactions such as a top decay to charged Higgs boson or new s-channels (heavy resonance, gravitons) in $t\bar{t}$ production have also been assessed.

Acknowledgements. This work has been performed within the ATLAS collaboration, and we thank collaboration members for helpful discussions. We are indebted to P. Uwer (CERN-TH) for long and fruitful discussions. We thank S. Bentvelsen (NIKHEF) for providing us with the W+4 jets events using AlpGen generator, and our colleague J.B. de Vivie de Regie (CPPM) for his help. Last but not least, we are grateful to W. Bernreuther and A. Brandenburg (RWTH) for their helpful collaboration.

References

1. M. Beneke et al., Top quark physics, CERN-TH-2000-100, hep-ph/0003033
2. D. Chakraborty, J. Konigsberg, D. Rainwater, Ann. Rev. Nucl. Part. Sci. **53**, 301 (2003), hep-ph/0303092
3. I. Bigi et al., Phys. Lett. B **181**, 157 (1986)
4. J.H. Kühn, Nucl. Phys. B **237**, 77 (1984)
5. V. Barger, J. Ohnemus, R.J.N. Phillips, Int. J. Mod. Phys. A **4**, 617 (1989)
6. G.L. Kane, G.A. Ladinsky, C.-P. Yuan, Phys. Rev. D **45**, 124 (1992)
7. F. Larios, E. Malkawi, C.-P. Yuan, Probing the electroweak symmetry breaking sector with the top quark, Talk given in July 1996 at CCAST Workshop, Beijing (China), hep-ph/9704288
8. J. Sjölin, J. Phys. G., Nucl. Part. Phys. **29**, 543 (2003); A. Brandenburg, J.P. Ma, Z. Phys. C **56**, 97 (1992); P. Haberl, O. Nachtmann, A. Wilch, Phys. Rev. D **53**, 4875 (1996), hep-ph/9505409
9. D. Atwood, A. Kagan, T.G. Rizzo, Phys. Rev. D **52**, 6264 (1995), hep-ph/9407408; R. Martinez, J.A. Rodriguez, M. Vargas, The anomalous chromomagnetic dipole moment of the top quark, hep-ph/9709478
10. E. Eichten, K. Lane, Phys. Lett. B **327**, 129 (1994), hep-ph/9401236
11. C.T. Hill, Phys. Lett. B **266**, 419 (1991); C.T. Hill, Phys. Lett. B **345**, 483 (1995), hep-ph/9411426
12. W. Bernreuther, A. Brandenburg, Phys. Lett. B **314**, 104 (1993); W. Bernreuther, A. Brandenburg, Phys. Rev. D **49**, 4481 (1994), hep-ph/9312210; W. Bernreuther, A. Brandenburg, M. Flesch, Phys. Lett. D **56**, 90 (1997), hep-ph/9701347; W. Bernreuther, M. Flesch, P. Haberl, Phys. Rev. D **58**, 114031 (1998), hep-ph/9709284
13. M. Arai et al. Phys. Rev. D **70**, 115015 (2004), hep-ph/0409273
14. M. Jezabek, J.H. Kühn, Phys. Lett. B **329**, 317 (1994), hep-ph/9403366; M. Jezabek, Nucl. Phys. Proc. Suppl. B **37**, 197 (1994), hep-ph/9406411
15. G. Malhon, S. Parke, Phys. Rev. D **53**, 4886 (1996), hep-ph/9512264
16. B. Gonzalez-Pineiro et al., Measuring V_{tb} and the polarization of top quarks and W bosons via boson gluon fusion at ATLAS, ATL-PHYS-2000-017
17. H.S. Do et al., Phys. Rev. D **67**, 091501 (2003), hep-ph/0209185
18. M. Beg et al., Phys. Rev. Lett. **38**, 1252 (1977); Erratum Phys. Rev. Lett. **39**, 54 (1977)
19. CDF Collaboration, Phys. Rev. D **71**, 031101 (2005); Erratum Phys. Rev. D **71**, 059901 (2005), hep-ex/0411070
20. CDF Collaboration, Phys. Rev. Lett. **84**, 216 (2000), hep-ex/9909042
21. D0 Collaboration, Phys. Lett. B **617**, 1 (2005), hep-ex/0404040
22. CDF Collaboration, Measurement of the W boson polarization in top quark decays using $\cos\Theta^*$ at CDF II, CDF/ANAL/TOP/PUB/7173; CDF Collaboration, A Measurement of the Fraction of Longitudinally-polarized W Bosons Produced in Top Quark Decays in $200\,pb^{-1}$ of $p\bar{p}$ Collisions at $\sqrt{s} = 1.96\,\mathrm{TeV}$, CDF note 7058; D0 Collaboration, Phys. Rev. D **72**, 011104 (2005)
23. A. Czarnecki, M. Jezabek, J.H. Kühn, Nucl. Phys. B **351**, 70 (1991)
24. A. Brandenburg, Z.G. Si, P. Uwer, Phys. Lett. B **539**, 235 (2002), hep-ph/0205023
25. G. Guillian, M. Campbell, D. Amidei, The choice of measurements for studying the top quark decay product angular distribution, CDF/ANAL/TOP/CDFR/4262
26. W. Bernreuther, A. Brandenburg, P. Uwer, Phys. Lett. B **368**, 153 (1996), hep-ph/9510300
27. P. Uwer, Phys. Lett. B **609**, 271 (2005), hep-ph/0412097
28. C. Benchouk, L. Hinz, E. Monnier, Top-Antitop spin correlation measurement in the semileptonic decay channel in the ATLAS experiment, ATL-PHYS-2002-024
29. W. Bernreuther et al., Nucl. Phys. B **690**, 81 (2004), hep-ph/0403035
30. W. Bernreuther et al., Phys. Rev. Lett. **87**, 242002 (2001), hep-ph/0107086
31. K. Smolek, V. Simak, Measurement of spin correlations of the top-antitop pairs in the ATLAS experiment, ATL-PHYS-2003-012

32. F. Hubaut, E. Monnier, P. Pralavorio, ATLAS sensitivity to $t\bar{t}$ spin correlation in the semileptonic channel, ATL-PHYS-PUB-2005-001
33. R. Bonciani et al., Nucl. Phys. B **529**, 424 (1998), hep-ph/9801375
34. S.R. Slabospitsky, L. Sonnenschein, Comput. Phys. Commun. **148**, 87 (2002), hep-ph/0201292
35. S. Frixione, B. Webber, The MCatNLO 2.3 Event Generator, hep-ph/0402116
36. H.L. Lai et al., Eur. Phys. J. C **12** 375, hep-ph/9903282
37. T. Sjöstrand et al., PYTHIA 6.2, Physics and Manual, LU-TP-01-21, hep-ph/0108264
38. A. Moraes, C. Buttar, I. Dawson, Prediction for Minimum Bias and the Underlying Event at LHC Energies, ATL-PHYS-PUB-2005-007
39. P. Golonka et al., The tauola-photos-F environment for the TAUOLA and PHOTOS packages, release II, CERN-TH/2003-287, hep-ph/0312240
40. M.L. Mangano et al., JHEP07, 001 (2003), hep-ph/0206293
41. B. Kersevan, E. Richter-Was, The Monte Carlo Event Generator AcerMC version 2.0 with interfaces to PYTHIA 6.2, HERWIG 6.5 and ARIADNE 4.1, TPJU-6-2004, hep-ph/0405247
42. E. Richter-Was, D. Froidevaux, L. Poggioli, ATLFAST 2.0 a fast simulation package for ATLAS, ATL-PHYS-98-131
43. ATLAS Collaboration, ATLAS Detector and Physics Performance Technical Design Report, CERN/LHCC 99-14
44. S. Corréard et al., b-tagging with DC1 data, ATL-PHYS-2004-006
45. S. Eidelman et al., Phys. Lett. B **592**, 1 (2004)
46. P. Roy, Perspectives de mesure de la masse du quark top avec le détecteur ATLAS, PHD thesis, Blaise Pascal University, PCCFT0202 (2002)
47. I. Borjanovic et al., Eur. Phys. J. C **39 S2**, 63 (2005), hep-ex/0403021
48. V. Simak et al., Reconstruction of top-antitop system from 2 leptons and 2 jets final states in experiment ATLAS, ATL-PHYS-2001-018
49. J. Pumplin et al., JHEP **0207**, 12 (2002), hep-ph/02011095
50. A.D. Martin et al., Phys. Lett. B **531**, 216 (2002), hep-ph/0201127
51. M. Gluck, E. Reya, A. Vogt, Eur. Phys. J. C **5**, 461 (1998), hep-ph/9806404
52. CDF Collaboration, Phys. Rev. D **63**, 032003 (2001), hep-ph/0006028
53. E. Ben-Haim, Eur. Phys. J. C **33**, 460 (2004)
54. D. Abbaneo et al., Phys. Rep. **294**, 1 (1998)
55. G. Corcella et al., JHEP01, 010 (2001), hep-ph/0011363
56. R. Hall, Top quark studies and searches for new phenomena at the Tevatron, talk given at the SLAC Summer Institute 2000, Stanford, August 2000
57. B.J. Kilminster, A search for non-Standard Model W helicity in top quark decays, CDF PhD Thesis (2003). Unpublished
58. N. Vickey, Measurement of W boson polarization in top quark decay, PhD Thesis, FERMILAB-THESIS-2004-49 (2004)
59. D. Chakraborty, Top quark and W/Z results from the Tevatron, Talk given in March 2002 at 37th Rencontres de Moriond on QCD and Hadronic Interactions, Les Arcs (France), hep-ex/0212027
60. F. del Aguila, J.A. Aguilar-Saavedra, Phys. Rev. D **67**, 014009 (2003), hep-ph/0208171
61. J. Cao et al., Phys. Rev. D **68**, 054019 (2003), hep-ph/0306278
62. Y. Min Nie et al., Phys. Rev. D **71**, 074018 (2005), hep-ph/0501048
63. X.-L. Wang, Q.-L. Zhang, Q.-P. Qiao, Phys. Rev. D **71**, 0140035 (2005), hep-ph/0501145
64. N. Mahajan, Phys. Rev. D **68**, 095001 (2003), hep-ph/0304235
65. E. Malkawi, C.P. Yuan, Phys. Rev. D **50**, 4462 (1994), hep-ph/9405322
66. R.D. Peccei, X. Zhang, Nucl. Phys. B **337**, 269 (1990)
67. W. Bernreuther et al., Nucl. Phys. B **388**, 53 (1992); Erratum Nucl. Phys. B **406**, 516 (1993)
68. C.-R. Chen, F. Larios, C.-P. Yuan, General Analysis of Single Top Production and W helicity in top decay, hep-ph/0503040
69. F. Hubaut, E. Monnier, P. Pralavorio, Measurement of the W polarization in top decays with semileptonic $t\bar{t}$ events, ATL-PHYS-PUB-2005-012
70. E. Boos, L. Dudko, T. Ohl, Eur. Phys. J. C **11**, 473 (1999), hep-ph/9903215
71. D. Espriu, J. Manzano, Phys. Rev. D **66**, 114009 (2002), hep-ph/0209030; D. Espriu, J. Manzano, Phys. Rev. D **65**, 073005 (2002), hep-ph/0107112
72. T. Hurth, Rev. Mod. Phys. **75**, 1159 (2003), hep-ph/0212304
73. F. Larios, M.A. Perez, C.-P. Yuan, Phys. Lett. B **457**, 334 (1999), hep-ph/9903394
74. B. Abbott et al., Phys. Rev. Lett. **85**, 256 (2000), hep-ex/0002058
75. T. Stelzer, S. Willenbrock, Phys. Lett. B **374**, 169 (1996), hep-ph/9512292
76. K. Cheung, Phys. Rev. D **55**, 4430 (1997), hep-ph/9610368
77. N. Arkani-Hamed, S. Dimopoulos, G.R. Dvali, Phys. Lett. B **429**, 263 (1998), hep-ph/9803315; I. Antoniadis et al., Phys. Lett. B **436**, 257 (1998), hep-ph/9804398